ELISA tests was performed by Western blot analysis (15, 26). All patients underwent a full neurological evaluation, routine blood and urine studies, cranial magnetic resonance imaging or computed tomography, and nerve conduction studies. The clinical features and laboratory data are summarized in Table 1.

## Pathological Assessment of Sural Nerve Biopsy Specimens

Sural nerve biopsy was performed before the initiation of treatment in all patients, as previously described (27–29). Specimens were divided into 2 portions. The first was fixed in 2.5% glutaraldehyde in 0.125 mol/L cacodylate buffer (pH 7.4) and embedded in epoxy resin for morphometric and ultrastructural studies. The density of myelinated fibers was assessed in toluidine blue-stained semithin sections using a computer-assisted image analyzer (Luzex FS; Nikon, Tokyo, Japan). The densities of small and large myelinated fibers were calculated as previously described (27, 28). The remainder of the glutaraldehyde-fixed sample was processed for the teased-fiber study, in which at least 200 single fibers were isolated and analyzed as described (27, 30). The second portion of each specimen was fixed in 10% formalin and embedded in paraffin. Sections were cut by routine methods and stained with hematoxylin and eosin, Congo red, the Klüver-Barrera method, and the Masson trichrome method.

For electron microscopy (EM), epoxy resin–embedded specimens were cut into 70-nm ultrathin transverse and longitudinal sections. Ultrathin sections were contrasted by staining with uranyl acetate and lead citrate. Sections were viewed with a transmission electron microscope (H-7100; Hitachi). To assess the density of unmyelinated fibers, random EM photographs were taken at a magnification of 4,000× to cover the area of the ultrathin sections, as previously described (27, 28, 31). Fibers with WSM and structures of paranodal regions and Schmidt-Lanterman incisures in longitudinal sections were confirmed in more highly magnified photographs.

**TABLE 1.** Patient Characteristics

| | |
|---|---|
| Age at examination, years | 68.4 ± 7.4 (59–83) |
| Age at onset, years | 65.8 ± 7.1 (56–82) |
| Sex (male/female), no. | 12/3 |
| Amount of IgM, mg/dL | 697 ± 440 (244–1,794) |
| Light-chain kappa/lambda | 13/2 |
| CSF protein | 136 ± 108 (55–381) |
| Nerve conduction study (mean) | |
| MCV, m/s; DL, ms; CMAP, mV | |
| Median nerve | 39.2, 9.1, 6.1 (57.6, 3.4, 10.7) |
| Tibial nerve | 29.0, 12.5, 2.2 (46.9, 4.5, 10.9) |
| SCV, m/s; SNAP, μV | |
| Median nerve | 29.4, 3.6 (57.8, 23.5) |
| Sural nerve | 37.0, 0.75 (51.0, 11.5) |

Values are expressed as the number of patients, mean, or mean ± SD with the indicated ranges. Control values were obtained from 171 normal subjects and based on previously published reports.

CMAP, compound muscle action potential; CSF, cerebrospinal fluid; DL, distal latency; MCV, motor nerve conduction velocity; SCV, sensory nerve conduction velocity; SNAP, sensory nerve action potential.

Because the endoneurial area is often enlarged in patients with anti-MAG neuropathy, we evaluated the total number of sural nerve fibers as well as their densities (32). The total endoneurial area was assessed using an image analyzer (Luzex FS) when complete transverse sections of the sural nerve were obtained. To determine the total population per sural nerve cross section, the density was multiplied by the total endoneurial area from which the subperineurial space was subtracted. We obtained complete transverse sections of the sural nerve in 10 of the 15 patients and analyzed the total population per cross section in these patients.

Control samples were obtained from 5 age-matched patients who had no neurological diseases (4 men and 1 woman; age range, 66–76 years; mean ± SD, 72.4 ± 4.2 years). Specimens were processed in the same manner as for the patients with anti-MAG neuropathy.

## Widely Spaced Myelin

Widely spaced myelin is defined as an increase in the distance separating the intraperiod line. The criteria for WSM are one or more wraps of myelin with a regularly separated intraperiod line and an intact major dense line occurring at the outer or inner aspect of the myelin sheath or throughout its thickness. Uncompacted myelin, which separates major dense lines with or without separation of the intraperiod line, was excluded (33). At least 300 fibers were assessed to determine the frequency of WSM in the myelinated fibers.

## Assessment of Neurofilaments

To evaluate the axonal cytoskeleton of myelinated fibers, we measured the number of neurofilaments across the axon in longitudinal sections. Using EM photographs at a magnification of 50,000×, neurofilaments were counted in 1-μm widths that vertically intersected the axon. To verify the regional differences in neurofilament density, we assessed the internode, juxtaparanode, and paranode. At least 10 axons in each of these 3 regions were examined to calculate the mean number of neurofilaments in every case.

## Immunostaining

Serial 7-μm-thick transverse and longitudinal cryostat sections from fresh-frozen tissue of nerve biopsy samples were incubated with the following antibodies: goat affinity-purified antibody to human IgM (5Fc μ) (1:1000; ICN/Cappel, Aurora, OH), rabbit polyclonal anti-MAG antibody (1:100; Santa Cruz Biotechnology, Santa Cruz, CA), rabbit polyclonal antibody to complement product C3d (1:400; Abcam, Cambridge, MA), or mouse anti–C5b-9 antibody (anti–terminal complement complex [anti-TCC], 1:200; Dako, Carpinteria, CA), followed by Alexa Fluor donkey anti-goat IgG (H + L, 1:1000), Alexa Fluor goat anti-rabbit IgG (H + L, 1:1000), or Alexa Fluor goat anti-mouse IgG (H + L, 1:1000). The stained sections were examined and photographed with a confocal laser scanning microscope (μ radiance BIORAD, Nikon, Tokyo, Japan).

## Statistical Analyses

Quantitative patient data (mean ± SD) were compared with control values. Statistical analyses were performed using the Mann-Whitney U test, Pearson correlation coefficient analysis,

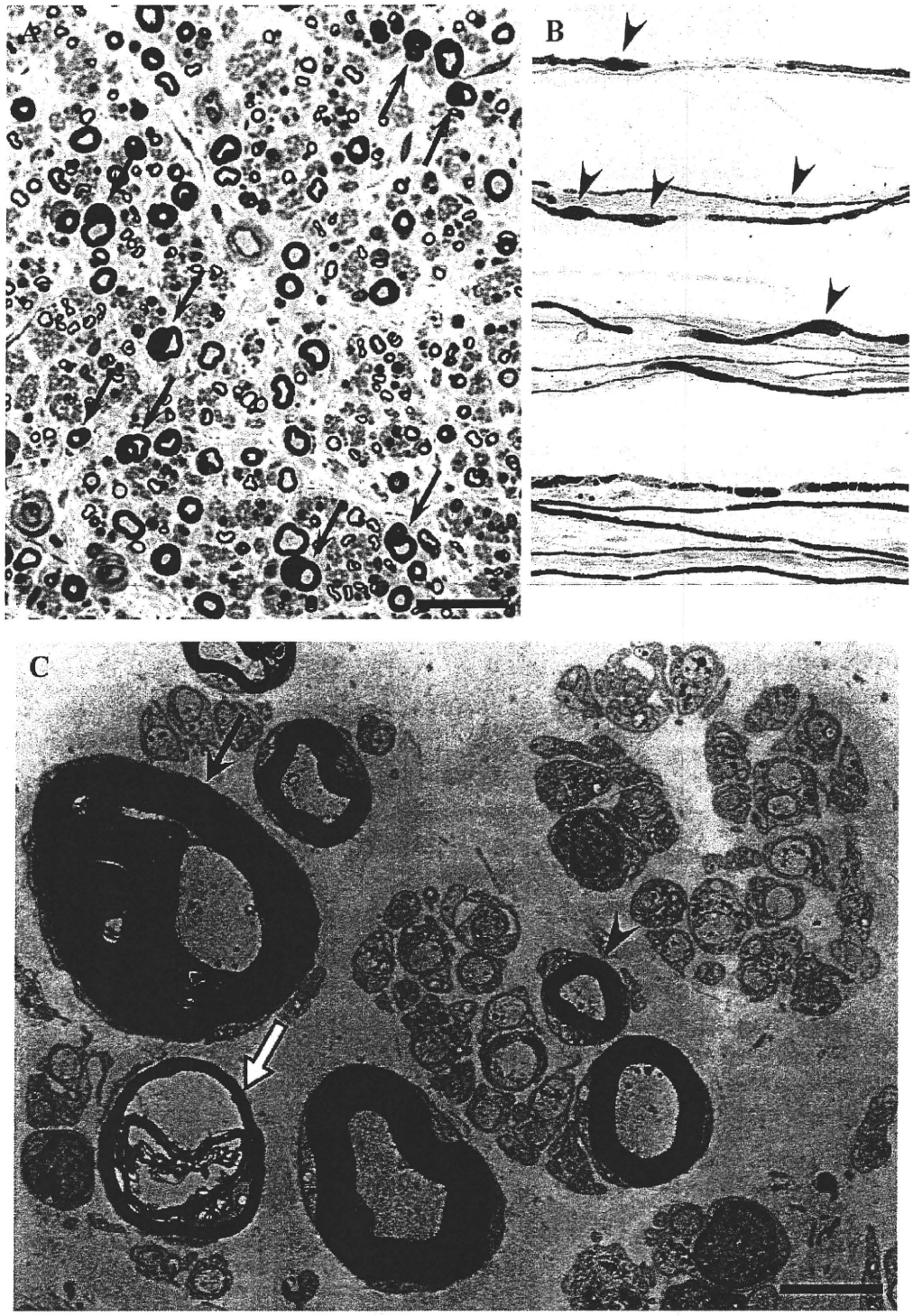


**FIGURE 1.** Sural nerve specimens from patients with anti–myelin-associated glycoprotein neuropathy. **(A)** Transverse section shows large myelinated fibers that are markedly reduced in number compared with small myelinated fibers; some fibers show axonal atrophy and focal myelin thickening (arrows). **(B)** Teased-fiber preparation shows segmental demyelination with tomaculous appearances (arrowheads) in both intermodal and paranodal regions and axonal degeneration. Fibers undergoing degeneration and remyelination are evident in the lowest section. **(C)** Electron micrograph of a transverse section. Unmyelinated nerve fibers are well preserved. There is a fiber with tomaculous appearance and axonal atrophy (arrow), axonal degeneration (white-filled arrow), and widely spaced myelin (arrowhead). Scale bars = **(A)** 20 μm; **(C)** 5 μm.

and Spearman regression analysis, as appropriate. Values of $p < 0.05$ were considered significant.

## RESULTS

### Light Microscopy

In semithin cross sections, myelinated fibers in IgM-MGUS anti-MAG neuropathy biopsies were decreased versus controls. Myelin sheaths often seemed inappropriately thick for the size of the axon (Fig. 1A). The total myelinated fiber densities were reduced by varying degrees (1,422–5,703 fibers/mm$^2$), especially in large myelinated nerve fibers (39% of the control mean of large fibers and 61% of the control mean of small fibers) (Table 2). In teased-fiber preparations, segmental demyelination/remyelination, tomaculous appearance, and axonal degeneration coexisted (Fig. 1B). The frequency of segmental demyelination/remyelination in the teased-fiber study was high (26.8% ± 9.9%), and axonal degeneration was also frequently seen (7.5% ± 4.1%) (Table 2). Tomacula, defined as myelin thickenings of more than 50% of the fiber diameter (34), and myelin irregularity were conspicuous. The frequency of fibers with tomacula was high in all patients (Table 2). Vasculitis, inflammation, and amyloid deposition in the endoneurium were not detected.

### Electron Microscopy

#### Transverse Sections

There were many demyelinating axons and remyelinating fibers with very thin myelin sheaths. Widely spaced myelin and tomaculous appearance with axonal atrophy were also frequent (Fig. 1C). Widely spaced myelin was observed in all patients and was preferentially located in the outer layers of the myelin sheath (Fig. 2A), whereas in some fibers, WSM involved the entire thickness of the myelin. Tomaculous appearance with redundant myelin loops and WSM frequently coexisted (Fig. 2B). Although the typical appearance of WSM consisted of several consecutive layers of separated intraperiod lines, separation of only the outermost layer with otherwise normal-appearing myelin was also found (Figs. 2C, D). There were redundant myelin loops with tomaculous appearance consisting of infolding (Fig. 2E) and outfolding (Fig. 2G). When the separation of only the outermost layer was considered, almost all redundant myelin loops were associated with WSM. Almost all fibers with tomaculous appearance also had WSM of only the outermost or a few outer layers (Figs. 2F, H).

The frequency of WSM in myelinated fibers varied from case to case (2.6%–46.8%, 12.5% ± 14.1%; Table 3) and was positively correlated with the frequency of demyelination and tomacula in the teased-fiber study ($p < 0.01$, $r = 0.46$ and $p < 0.01$, $r = 0.52$, respectively) and negatively correlated with the total myelinated fiber density ($p < 0.01$, $r = -0.43$) (Fig. 3). However, there was no correlation between the frequency of WSM and axonal degeneration in teased-fiber preparations.

In contrast to myelinated fibers, the unmyelinated fiber density was well preserved (Fig. 1C; Table 2). On the entire transverse section of the sural nerve, the number of unmyelinated fibers was almost the same as the normal control value (Table 2). Ballooning of axons, accumulation of specific organelles, and other morphological abnormalities suggesting damage to unmyelinated axons were not apparent in any case.

#### Longitudinal Sections

As in the transverse sections, WSM was found preferentially in the outer layers of the myelin sheath. In paranodal regions, spaces between terminal myelin loops, especially those adjacent to the node of Ranvier, were widened compared with normal myelinated fibers (Figs. 4A, B). This widening of the spaces between terminal myelin loops seemed to continue to juxtaparanodal regions (Fig. 4B). Progression of these morphological changes, especially adjacent to the node of Ranvier, seemed to lead to WSM in paranodal regions (Fig. 4C). Concomitant with this finding, some of the terminal myelin loops, especially those adjacent to the node of Ranvier, were swollen (Fig. 4D). Some swollen terminal myelin loops were detached from the paranodal axolemma and were in juxtaparanodal regions; these loops seemed to be retracted from the paranodal regions (Figs. 5A, B). This seemed to progress to widening of the node of Ranvier (i.e. demyelination) (Figs. 6A, B). Paranodal WSM, swelling of terminal myelin loops, and detachment between the terminal myelin loops and the paranodal axolemma were found in many cases (Table 3), and their frequencies seemed to correlate with the frequency of WSM in transverse sections ($p < 0.01$, $p < 0.05$, and $p < 0.05$, respectively). The frequency of WSM in the transverse sections also positively correlated with anti-MAG titers ($p < 0.01$) (Fig. 7). The degrees of pathological abnormalities in longitudinal sections (i.e. paranodal WSM, swelling of terminal myelin loops,

**TABLE 2.** Pathological Features in Patients With Anti–Myelin-Associated Glycoprotein Neuropathy

| | Anti-MAG Neuropathy (n = 15) | Control (n = 5) | |
|---|---|---|---|
| | Mean ± SD | Mean ± SD | p* |
| Myelinated fiber density, no./mm$^2$ | | | |
| Total | 3,601 ± 1,109 | 7,175 ± 1,227 | <0.005 |
| Large | 846 ± 468 | 2,426 ± 468 | <0.005 |
| Small | 2,755 ± 860 | 4,749 ± 872 | <0.01 |
| Total no. of myelinated fibers, no./nerve | | | |
| Total | 4,122 ± 1,615 | 7,481 ± 1,359 | <0.005 |
| Large | 947 ± 541 | 2,422 ± 460 | <0.005 |
| Small | 3,175 ± 1,218 | 5,059 ± 1,038 | <0.05 |
| Unmyelinated fiber density, no./mm$^2$ | 26,077 ± 2,507 | 30,468 ± 3,472 | NS |
| Total no. of unmyelinated fibers, no./nerve | 29,915 ± 4,379 | 31,647 ± 3,109 | NS |
| Teased-fiber preparation, % of fibers with | | | |
| Segmental demyelination/remyelination | 26.8 ± 9.9 | 12.4 ± 4.8 | <0.01 |
| Axonal degeneration | 7.3 ± 4.5 | 3.7 ± 1.8 | <0.05 |
| Tomaculous appearance | 15.9 ± 19.8 | 0 | — |

Control values (mean ± SD) are based on previously published reports.
*Determined using the Mann-Whitney U test.
MAG, myelin-associated glycoprotein; NS, not significant.

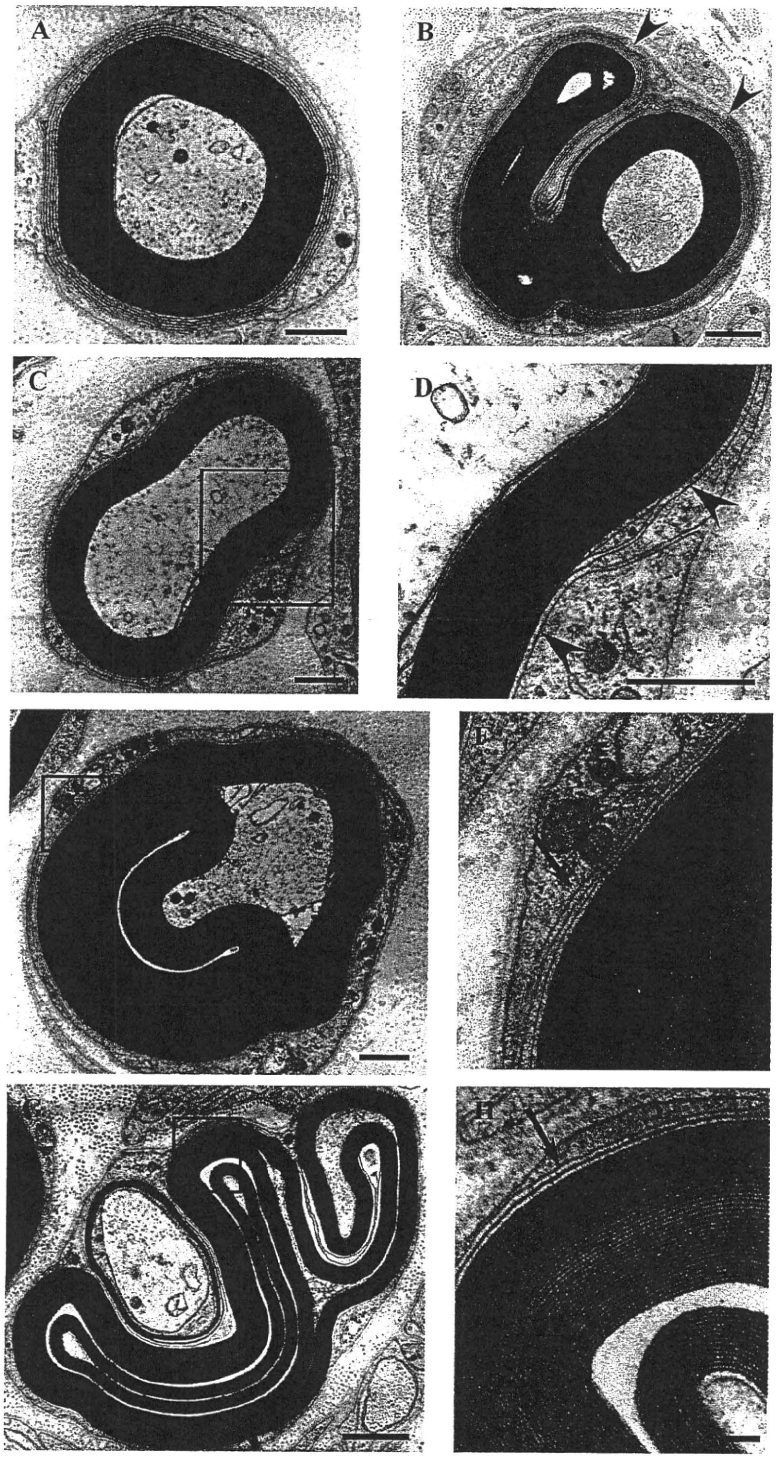


**FIGURE 2.** Electron micrographs of a transverse section. **(A)** Widely spaced myelin (WSM) in some outer lamellae of the myelin sheath. **(B)** Redundant myelin loops and WSM (arrowheads) in the outer layers. **(C)** Fibers with WSM in the outermost layer of the myelin sheath. **(D)** High-power micrograph of the boxed area in **(C)** shows WSM in the outermost layer in continuity with the outer mesaxon (arrowheads). **(E, G)** Redundant myelin loops with myelin infolding **(E)** and outfolding **(G)**; these features likely correspond to the tomacula seen in teased-fiber preparations. **(F, H)** High-power micrographs of the boxed areas in **(E)** and **(G)**, respectively, show WSM in the outermost or some outer layers (arrows). Scale bars = **(A–E)** 1 μm; **(F)** 0.1 μm; **(G)** 1 μm; **(H)** 0.1 μm.

**TABLE 3.** Pathological and Serological Data in Patients With Anti–Myelin-Associated Glycoprotein Neuropathy

| | | MAG Antigen Analysis | | Cross Sections | | | Longitudinal Sections | | | | |
|---|---|---|---|---|---|---|---|---|---|---|---|
| Case No. | Serum IgM, mg/dL | ELISA Titer | Western Blot | MF Density, no./mm$^2$ | Total No. UMF, no./nerve | Frequency of WSM, % | Swelling of TML | Paranodal WSM | Detachment Between TML and PA | SLI With WSM | Tomacula With WSM |
| 1 | 379 | 51,200 | + | 2,978 | 28,463 | 9.2 | +++ | + | ++ | ++ | +++ |
| 2 | 1,794 | 102,400 | + | 1,422 | — | 25.3 | +++ | +++ | +++ | +++ | +++ |
| 3 | 447 | 1,600 | + | 5,528 | 28,087 | 2.8 | + | + | 0 | + | + |
| 4 | 524 | 1,600 | + | 5,030 | 34,000 | 2.6 | + | + | 0 | + | + |
| 5 | 1,090 | 51,200 | + | 3,504 | 32,029 | 4.7 | ++ | ++ | + | + | + |
| 6 | 1,125 | 3,200 | + | 5,426 | 25,091 | 3.4 | + | + | 0 | + | + |
| 7 | 244 | 6,400 | + | 2,124 | — | 46.8 | ++ | ++ | + | ++ | +++ |
| 8 | ND | 1,600 | + | 4,306 | 21,886 | 3.0 | + | + | 0 | + | + |
| 9 | 312 | 1,600 | + | 4,162 | 35,656 | 3.2 | + | + | + | ++ | + |
| 10 | 253 | 1,600 | + | 5,703 | 34,183 | 2.7 | + | + | 0 | + | + |
| 11 | 653 | 1,600 | + | 3,198 | — | 10.9 | + | + | + | + | + |
| 12 | 576 | 12,800 | + | 2,213 | 27,997 | 19.1 | +++ | + | ++ | +++ | + |
| 13 | 437 | 6,400 | + | 3,614 | — | 13.5 | ++ | + | + | + | ++ |
| 14 | 1,030 | 409,600 | + | 3,465 | 31,775 | 38.5 | +++ | +++ | +++ | +++ | ++ |
| 15 | 890 | 6,400 | + | 3,443 | — | 3.7 | + | + | 0 | + | + |

Lesions in nerve fibers in longitudinal sections were graded: +++ = many typical lesions; ++ = moderate number of typical lesions; + = few typical lesions; 0 = no lesions.
MAG, myelin-associated glycoprotein; MF, myelinated fiber; ND, not determined; PA, paranodal axolemma; SLI, Schmidt-Lanterman incisure; TML, terminal myelin loops; UMF, unmyelinated fiber; WSM, widely spaced myelin.

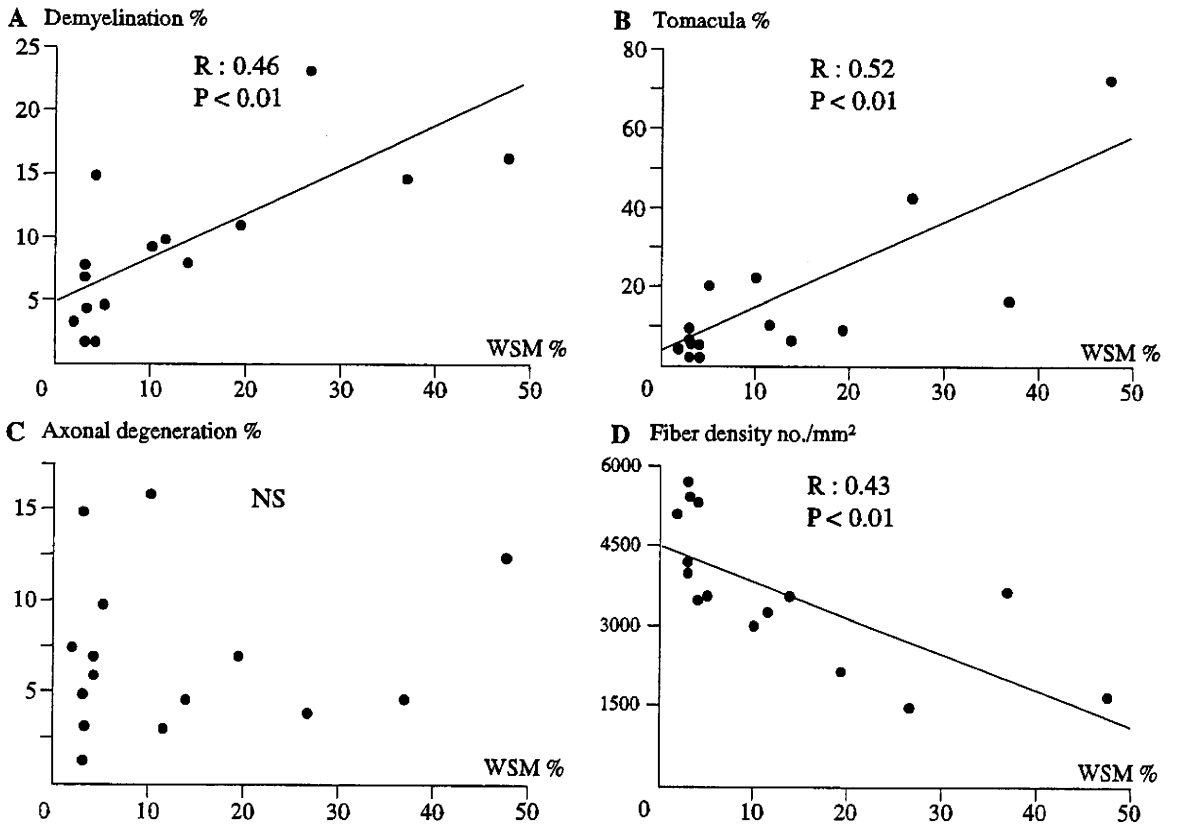


**FIGURE 3.** Correlations between the frequency of widely spaced myelin (WSM) and teased-fiber appearances. **(A–D)** Bold lines represent regression lines. The frequencies of demyelination **(A)**, tomacula **(B)**, and decreases in total myelinated fibers **(D)** show a positive correlation with WSM. There is no correlation between axonal degeneration and the frequency of WSM **(C)**. NS, not significant.

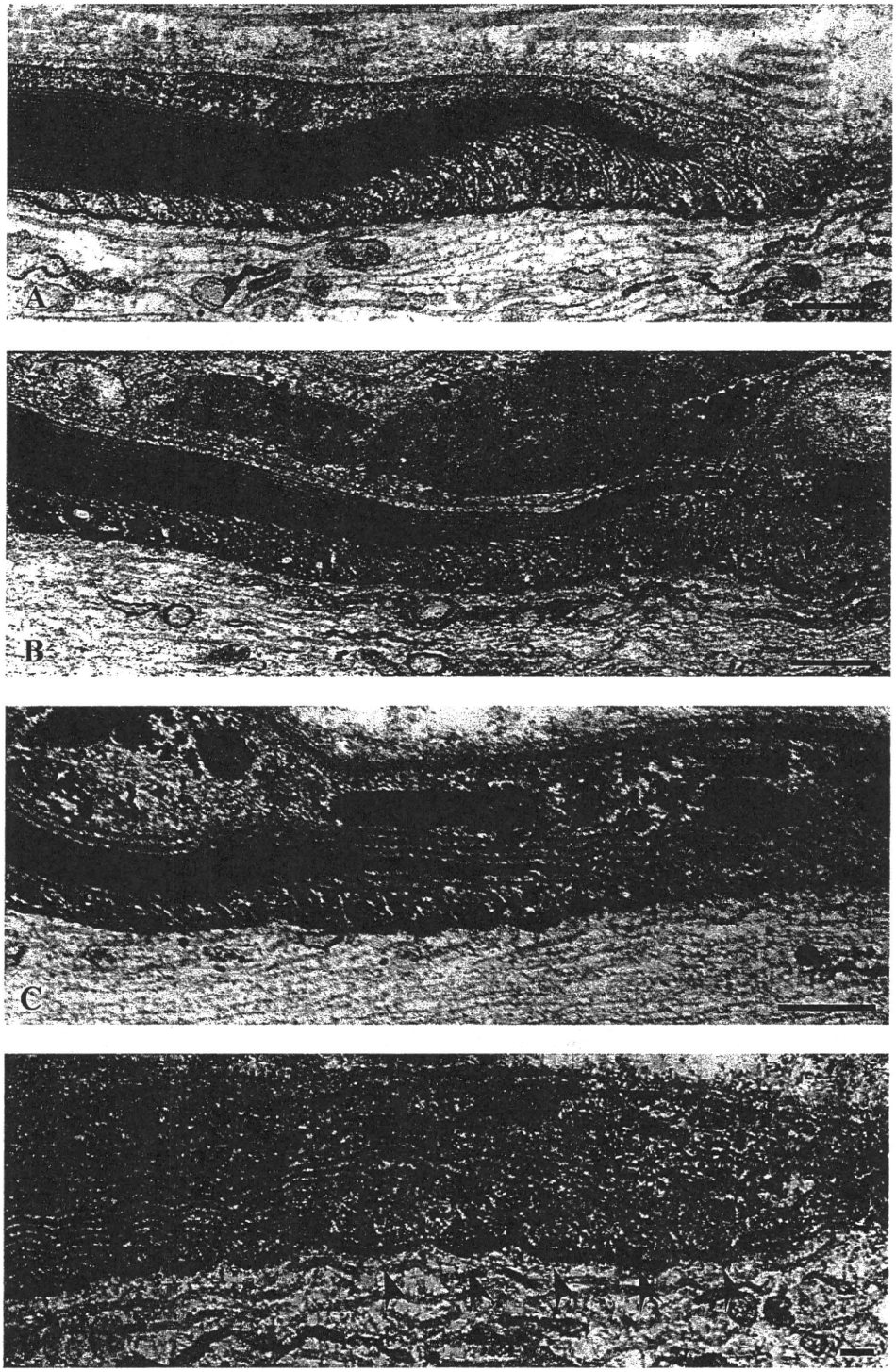


**FIGURE 4.** Electron micrographs of longitudinal sections in the paranodal region of nerve biopsy specimens from a normal control **(A)** and from patients with anti–myelin-associated glycoprotein neuropathy **(B–D)**. **(B)** There is widening of spaces between terminal myelin loops (arrows) that continues to the juxtaparanodal region and widely spaced myelin (WSM) in the outermost lamellae (arrowhead). **(C)** As in **(B)**, there is widening of spaces between terminal myelin loops (arrows); some outer terminal myelin loops are slightly swollen, and there is WSM in some outer layers (arrowheads). **(D)** High-power detail of terminal myelin loops adjacent to the node of Ranvier. Spaces between terminal myelin loops are widened, and outer terminal myelin loops seem swollen (arrowheads). Scale bars = **(A–C)** 0.5 μm; **(D)** 0.1 μm.

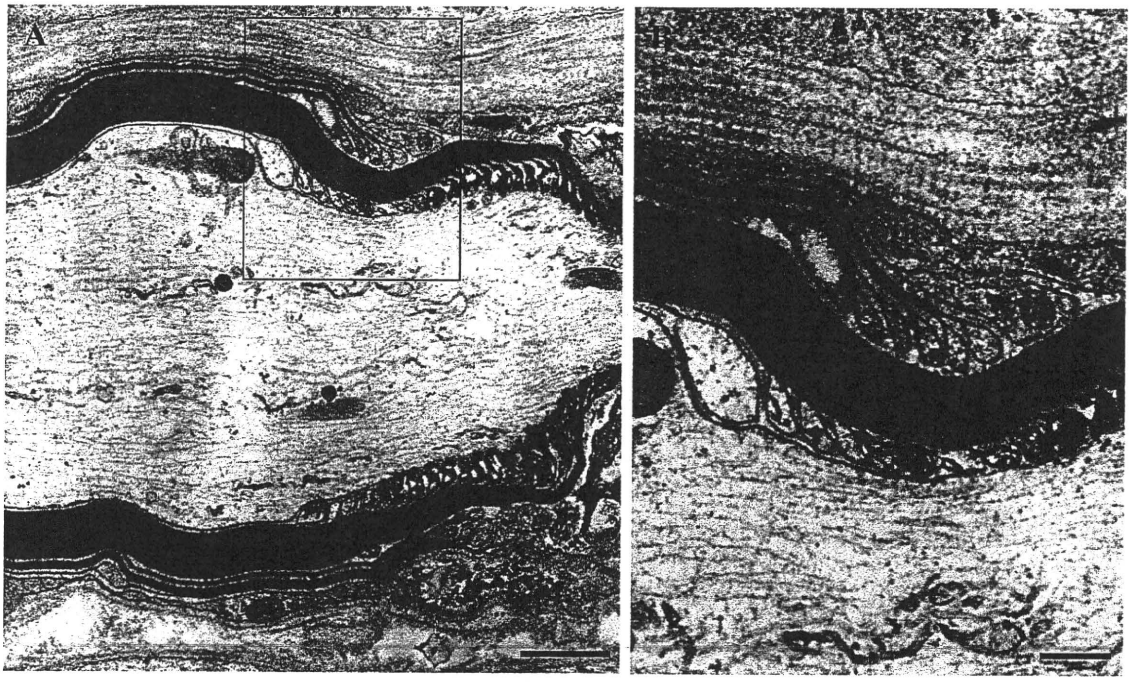


**FIGURE 5.** Longitudinal section from another node from a case of anti–myelin-associated glycoprotein neuropathy. **(A)** Electron micrograph shows detachment between outer terminal myelin loops and paranodal axolemma. Widely spaced myelin (WSM) is in continuity from the paranodal region. **(B)** Detail of the boxed area in **(A)** shows that outer terminal myelin loops with WSM retract from the paranodal region. Scale bars = **(A)** 0.5 μm; **(B)** 0.1 μm.

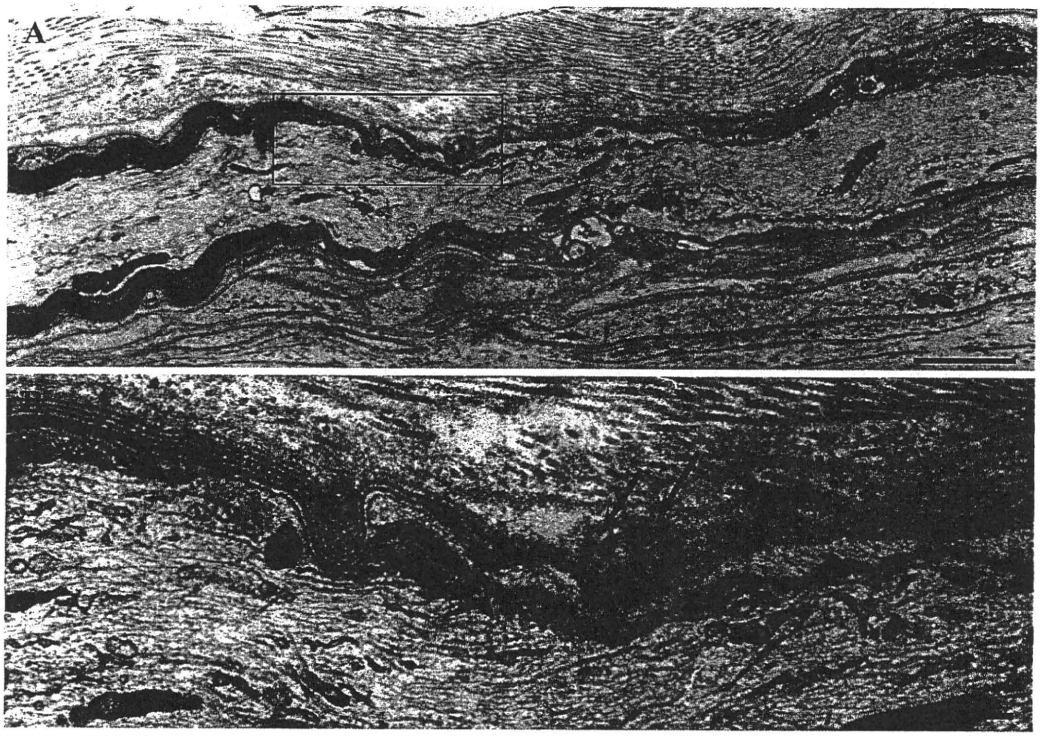


**FIGURE 6.** Longitudinal section from a case of anti–myelin-associated glycoprotein neuropathy. **(A)** Electron micrograph shows extensive demyelination. **(B)** Detail of the boxed area in **(A)** shows 2 terminal myelin loops that are dissociated from the paranodal axolemma (arrows). Scale bars = **(A)** 1 μm; **(B)** 0.5 μm.

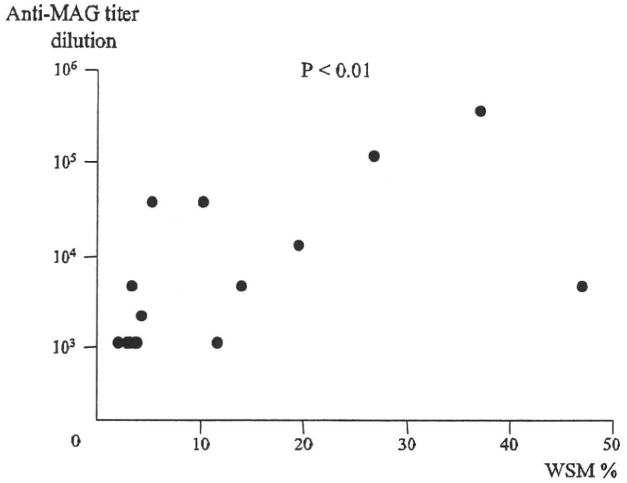


**FIGURE 7.** Correlation between anti–myelin-associated glycoprotein (MAG) titers and frequency of widely spaced myelin (WSM) in transverse sections. The frequency of WSM in transverse sections is positively correlated with anti-MAG titers ($p < 0.01$, Spearman rank correlation analysis).

and tomacula with WSM) were also correlated with anti-MAG titers ($p < 0.05$, $p < 0.005$, and $p < 0.05$, respectively). On the other hand, serum IgM levels did not correlate with either anti-MAG titers or pathological indices (Table 3). In addition to the association of paranodal terminal myelin loops with WSM, Schmidt-Lanterman incisures with WSM were also frequently observed (Figs. 8A, B; Table 3), but demyelination was not observed in these areas.

Tomacula were observed in both paranodal and internodal regions on longitudinal sections in all cases (Figs. 9A, B; Table 3). As in the transverse sections, almost all fibers with tomacula had WSM, especially in the outer layers of the myelin sheath (Figs. 9C, D). Large tomacula with complex redundant myelin loops in juxtaparanodal regions were also associated with widening of the node of Ranvier (i.e. demyelination).

Neurofilament densities in the axons in longitudinal sections were significantly greater in neuropathy versus normal control biopsies (number of filaments per micrometer, $13.9 \pm 3.2$ vs $9.8 \pm 3.4$ for paranode, $p < 0.01$; $12.7 \pm 2.2$ vs $9.0 \pm 1.9$ for juxtaparanode, $p < 0.05$; $10.2 \pm 1.5$ vs $7.5 \pm 1.4$ for internode, $p < 0.05$) (Fig. 10A). The increase in neurofilament density was most prominent in paranodal regions (Figs. 10A–C).


**FIGURE 8.** Electron micrographs of longitudinal sections of Schmidt-Lanterman incisures in specimens from a normal control **(A)** and anti–myelin-associated glycoprotein neuropathy **(B)**. Widely spaced myelin is in continuity with Schmidt-Lanterman incisures. Scale bars = 0.5 μm.

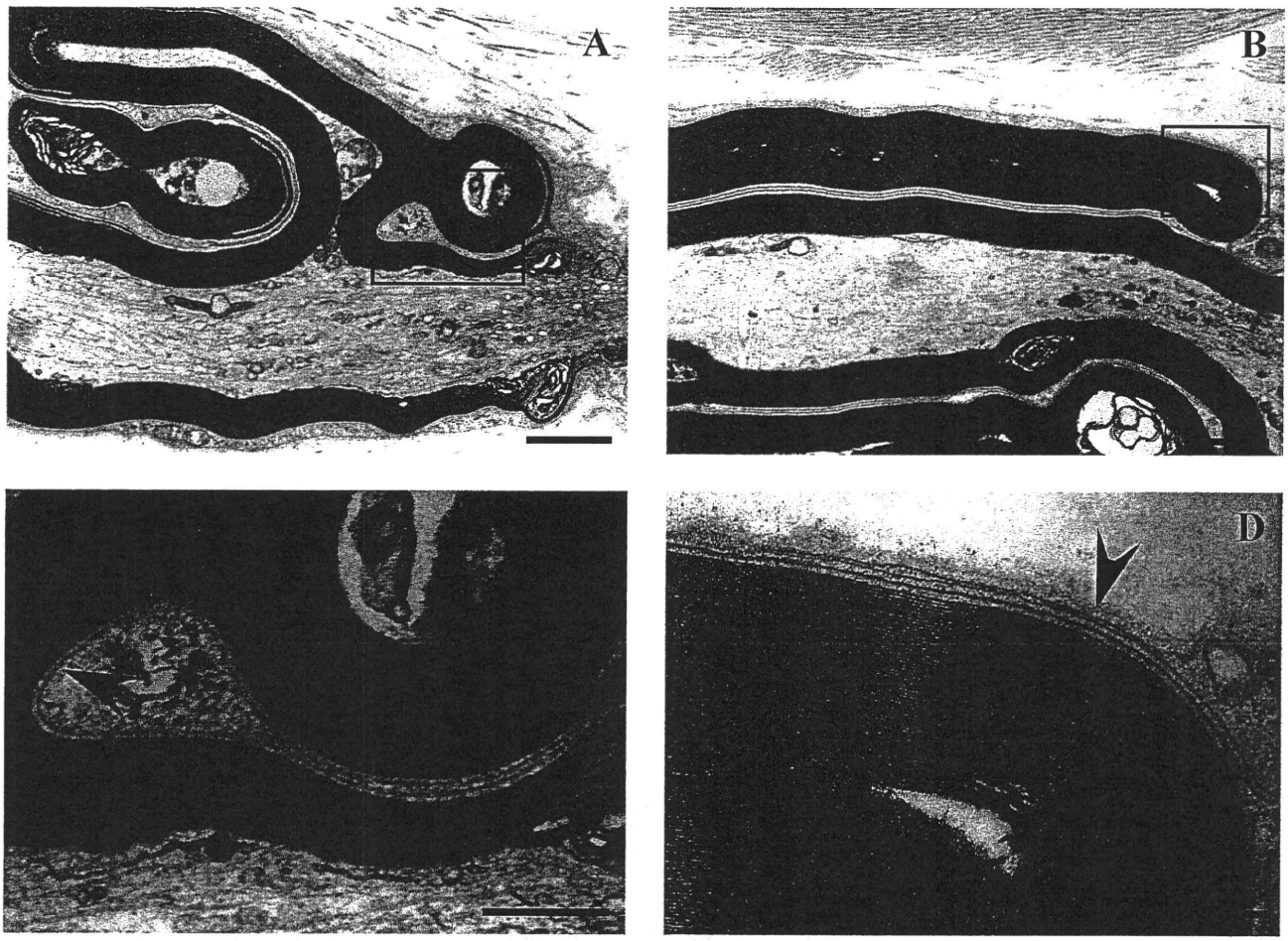


**FIGURE 9.** Electron micrograph of a longitudinal section at the paranodal and internodal regions showing tomaculous appearances. **(A, B)** Tomacula are observed in both paranodal **(A)** and internodal regions **(B)**. **(C, D)** High-power details of the boxed areas in **(A)** and **(B)** show widely spaced myelin in the outermost or some outer layers (arrowheads). Scale bars = **(A, B)** 1 μm; **(C, D)** 0.5 μm.

### Immunofluorescence Staining

Indirect immunofluorescence was performed on cross sections and longitudinal sections in all cases. In cross sections, the MAG staining pattern was ringlike, corresponding to the periaxonal membrane, or double-line rings, corresponding to both the periaxonal membrane and Schmidt-Lanterman incisures. The IgM antibody deposits were present on both large and small myelinated nerve fibers (Fig. 11A). They appeared as either a thin line at the periphery of myelinated fibers or rings in the inner layer of the myelin sheath, corresponding to Schmidt-Lanterman incisures. In longitudinal sections, IgM deposits were continuous along the outermost layer of the myelin sheath and were concentrated at both paranodal regions and Schmidt-Lanterman incisures (Fig. 11B). These areas were consistent with those that showed WSM. No IgM deposit was seen on the periaxonal membrane on longitudinal sections. Immunoglobulin M and MAG were colocalized in paranodal regions and Schmidt-Lanterman incisures. Confocal microscopic analysis revealed colocalization of IgM and C3d (Figs. 11C–E), although C5b-9 (anti-TCC) was not observed on the myelin sheath.

## DISCUSSION

Characteristic morphological changes in anti-MAG neuropathy include WSM, demyelination, axonal atrophy, and tomaculous appearance of myelinated fibers (15, 19, 20, 22, 23), and were found in all cases in our series. The pathogenic role of anti-MAG antibodies in this neuropathy has been investigated with passive immunization or systemic transfusion of anti-MAG IgM antibody into animals and was shown to cause WSM and myelin destruction (11, 35, 36). Immunoelectron microscopy demonstrated the selective presence of monoclonal IgM at the sites of myelin widening in patients with IgM monoclonal anti-MAG neuropathy (24). Thus, WSM is considered to be caused by direct binding of IgM to the myelin membrane, leading to abnormal myelin spacing (21, 37). However, it is still unclear how WSM develops morphologically and how its development correlates with the other characteristic findings in anti-MAG neuropathy. In this study, we demonstrated (*a*) a positive correlation between the frequency of WSM and demyelination and tomacula and the degree of reduction of myelinated fibers, (*b*) close association of WSM

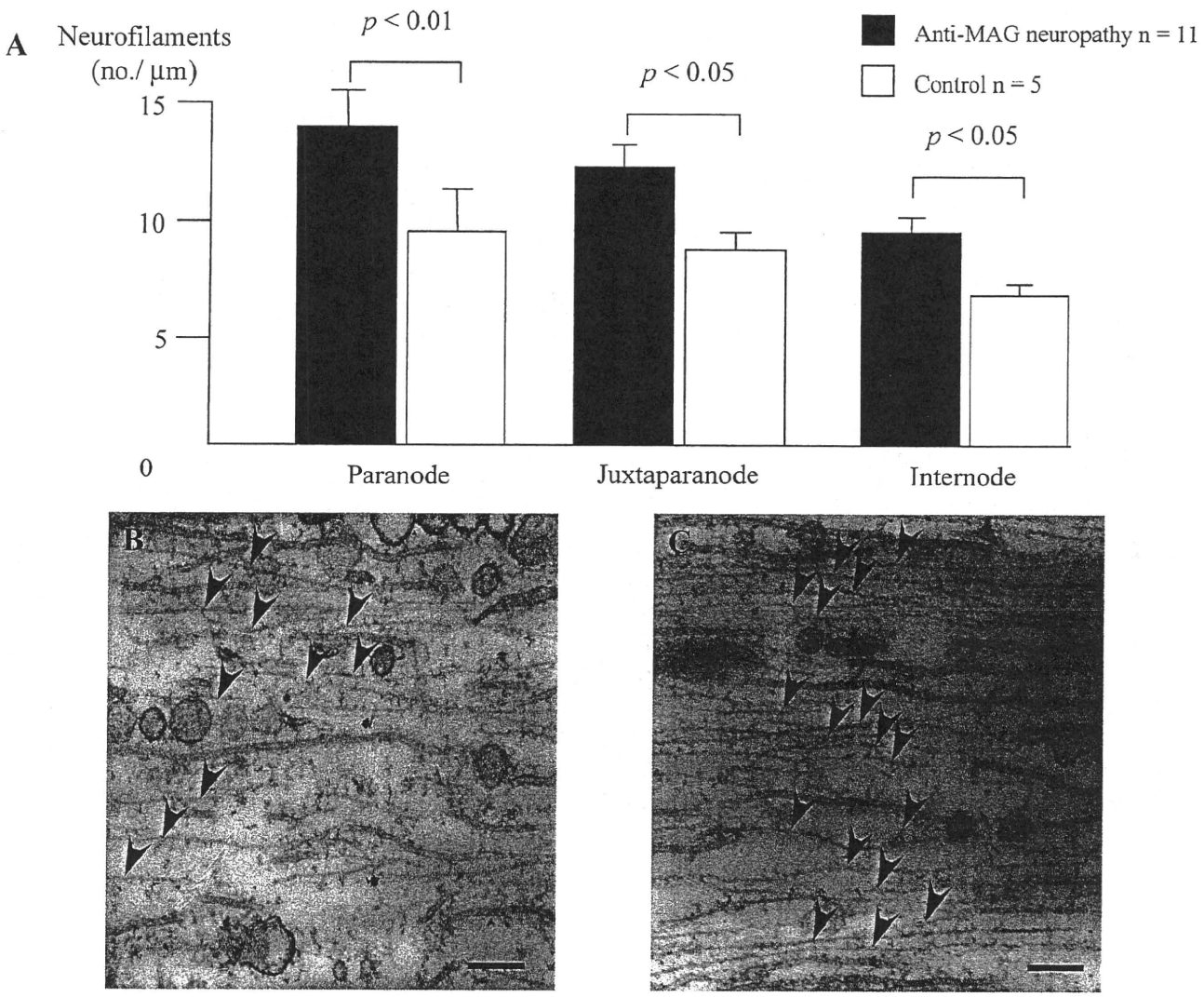


**FIGURE 10.** Neurofilament density in longitudinal sections. **(A)** The number of neurofilaments is significantly greater in patients with anti–myelin-associated glycoprotein (MAG) neuropathy versus normal controls. **(B, C)** Electron micrographs of longitudinal sections of the paranodal region. The neurofilaments (arrowheads) in anti-MAG neuropathy **(C)** are denser than those in the normal control **(B)**. Scale bars = **(B, C)** 0.2 μm.

with redundant myelin loops with tomaculous appearance, (*c*) widening of the spaces between terminal myelin loops accompanied by their swelling as an early morphological change before demyelination, (*d*) the highest neurofilament density at paranodal regions, and (*e*) coincidence of areas with WSM and IgM deposition.

Our EM studies of longitudinal sections demonstrated that WSM developed in relation to the node of Ranvier, the outer layer of the myelin sheath, and Schmidt-Lanterman incisures. Immunofluorescence studies demonstrated positive staining of anti-IgM antibody in these areas. Previous studies have also reported that MAG is located on noncompact myelin such as paranodal loops and Schmidt-Lanterman incisures (38–40). The MAG plays a role in adhesion between Schwann cell membranes in paranodal regions and Schmidt-Lanterman incisures; thus, dysfunction of the adhesive properties of MAG may lead to the unique morphological changes seen at those sites (41). In this context, the widening of the spaces between terminal myelin loops we observed may be one of the earliest changes that occur at the paranodal region. This widening may cause formation of WSM at paranodal regions and eventually lead to impairment of adhesion between myelin terminals and paranodal axolemma. Detachment of swollen terminal myelin loops from the paranodal axolemma may occur when widening occurs in the space between terminal myelin loops, and these morphological changes may be associated with demyelination at the node of Ranvier (Figs. 12A–E). The detachment may be further accelerated by loosening of myelin sheaths caused by WSM in the outer layer of the myelin sheath. Detachment of outer layers may enhance the retraction

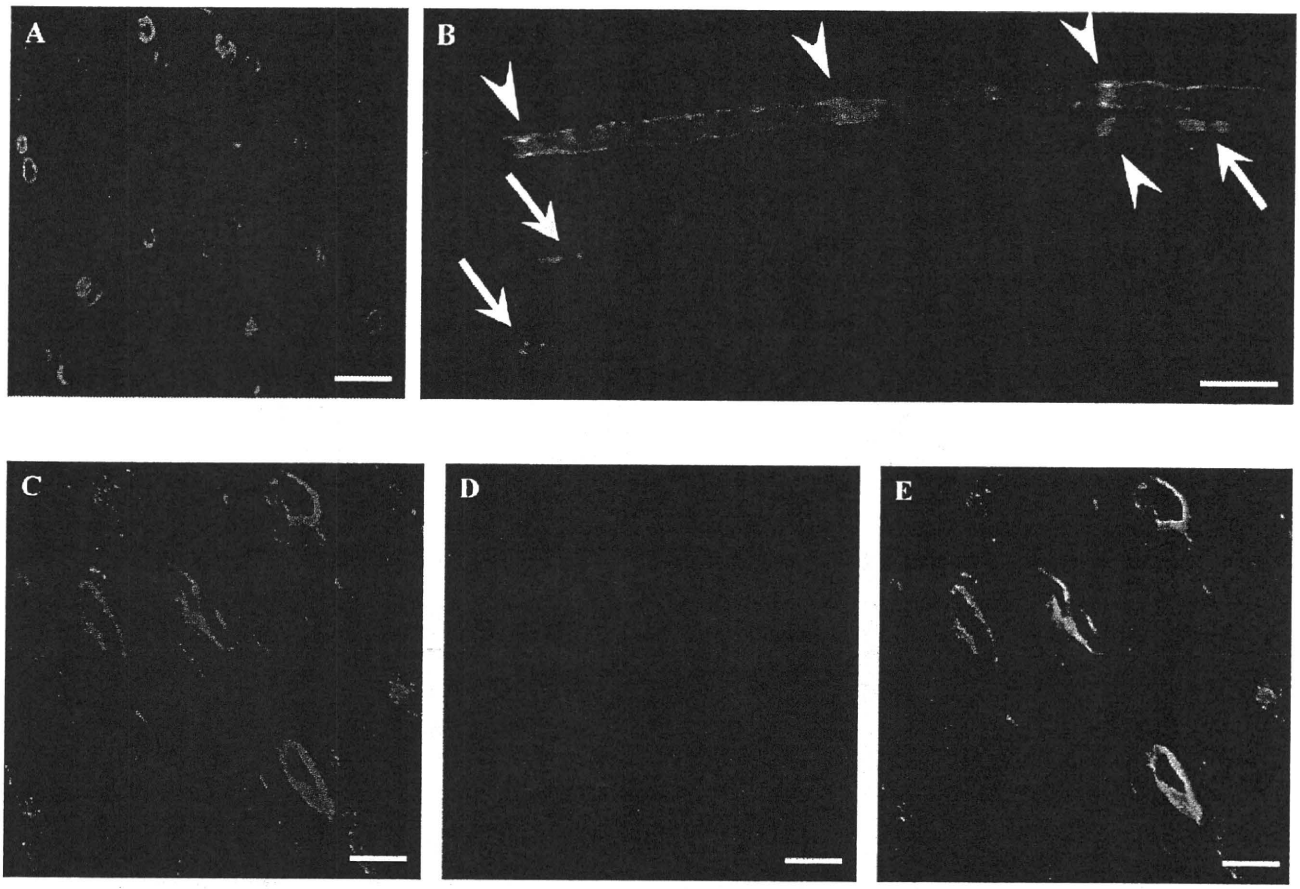


**FIGURE 11.** Immunofluorescence with anti-IgM antibody (green) on cross sections **(A)** and longitudinal sections **(B)** in anti-myelin-associated glycoprotein neuropathy. Immune reaction with the anti-IgM antibody is concentrated both in paranodal regions (arrows) and Schmidt-Lanterman incisures (arrowheads). Immunoglobulin M is also seen along the outermost layer of the myelin sheath. **(C–E)** Confocal microscopy reveals colocalization (yellow) in the merged image **(E)** of IgM (green) **(C)** and C3d (red) **(D)**. Scale bars = **(A, B)** 10 μm; **(C–E)** 3 μm.

of terminal myelin loops and lead to the widening of the node of Ranvier and subsequent demyelination. These observations were strongly supported by our immunohistochemical study and the correlation between the frequency of WSM and demyelination in teased fibers (Fig. 3). Furthermore, serum anti-MAG antibody titers were clearly correlated with the frequency of WSM in transverse sections and early pathological changes at the node of Ranvier. Together, our observations strongly suggest that anti-MAG antibodies induce WSM, other myelin changes, and subsequent demyelination and tomaculous formation.

In teased fibers and by EM, almost all tomacula with redundant myelin loops were accompanied by WSM. Because tomacula were found in both paranodal and internodal regions, loosening of myelin sheaths caused by WSM in the outer layer of the myelin sheath may be important in the formation of tomacula.

We confirmed the coexistence of both IgM and the complement component C3d, in paranodal regions and Schmidt-Lanterman incisures, as previously reported (42–45). Previous studies have suggested that the complement pathway, including the TCC, is the effector of myelin changes in neuropathy associated with IgM monoclonal gammopathy (43) and experimental autoimmune neuritis (46). However, another study suggested that TCC may not be required for the breakdown of myelin components, or that the mechanism of IgM penetration into myelinated fibers through destruction of the basement membrane may not be mediated by TCC (45). We did not observe the TCC on myelin sheaths and, because of the slow progression in anti-MAG neuropathy that evolves during many years, the role of the complement pathway in anti-MAG neuropathy may be different from that in acute inflammatory demyelinating neuropathies in which TCC actively participates. Although active involvement of the complement pathway in the pathogenesis of anti-MAG neuropathy is still unclear, our finding that deposits of IgM and C3d were colocalized in the paranodal region suggests that the IgM antibody might injure myelin through activation of the complement pathway. Further investigation, including immunoelectron microscopy, may clarify the relationship between myelin alterations and the involvement of the complement pathway (24, 25, 47, 48).

In addition to paranodal loops and Schmidt-Lanterman incisures, MAG is also located on periaxonal membranes

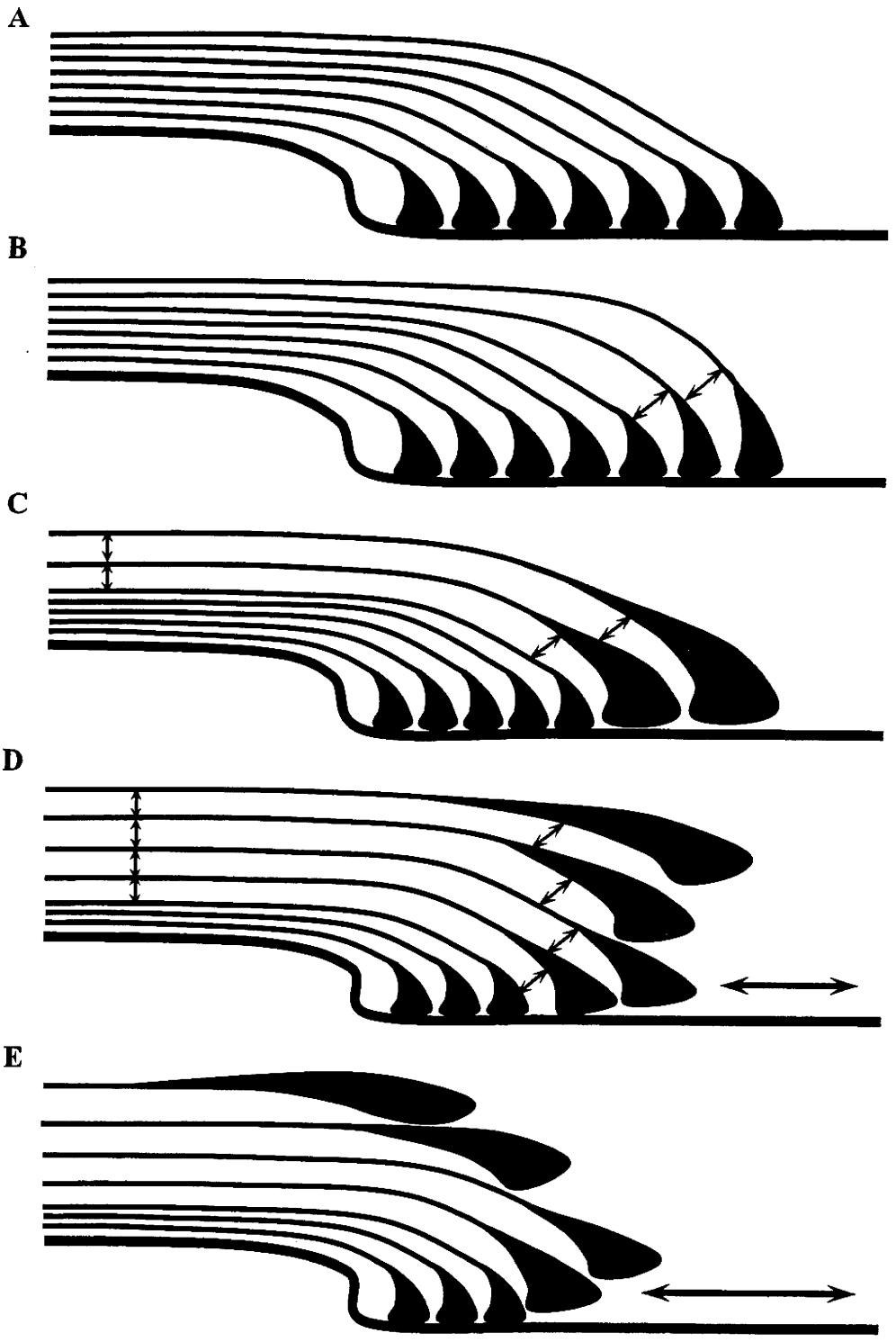


**FIGURE 12.** Schematic representation of the progression of demyelination in anti–myelin-associated glycoprotein neuropathy. **(A)** Relationship between myelin terminals and paranodal axolemma in longitudinal sections of normal myelinated fibers. **(B)** Widening of spaces between myelin terminals. **(C)** Progression of the widening of spaces between terminal myelin loops with conspicuous swelling constitutes widely spaced myelin (WSM). **(D)** Some of these terminal myelin loops with conspicuous swelling are detached from the paranodal axolemma **(E)**. Detachment may be further accelerated by the loosening of myelin sheaths caused by WSM, leading to widening of the node of Ranvier.

(38–40). The MAG in the periaxonal membrane plays a role in axon–Schwann cell signaling; the axon caliber of myelinated fibers in MAG-deficient mice is reduced because of decreased neurofilament phosphorylation (49–52). Consequently, dysfunction of MAG on the periaxonal side leads to an increase in neurofilament density and axonal atrophy, resulting in myelin collapse. However, we did not observe immunostaining for IgM or C3d in the periaxonal membrane, although MAG was located at that site. This finding might be caused by inaccessibility of the IgM antibody to the periaxonal membrane. We found that the neurofilament density was significantly increased in paranodes, juxtaparanodes, and internodes in anti-MAG neuropathy, with the highest density in the paranode. This suggests that axonal damage may be most severe in this region, and that axonal damage is initiated in paranodal regions where the initial stages of demyelination occur. Therefore, demyelination caused by detachment of terminal myelin loops from paranodal axolemma may be the primary cause of axonal atrophy and subsequent axonal damage in this neuropathy. Although the presence of MAG in unmyelinated fibers was not assessed, the preservation of unmyelinated fibers (in contrast to myelinated fibers) supports the view that demyelination is the primary cause of axonal damage in this neuropathy.

In summary, we demonstrated the close relationship between WSM and demyelination and tomacula. We suggest that the pathology occurring in myelin terminals in paranodal regions, which may be caused by activation of the complement pathway, results in extensive demyelination and subsequent axonal damage in anti-MAG neuropathy.

## REFERENCES


1. Kelly JJ Jr. Peripheral neuropathies associated with monoclonal proteins: A clinical review. Muscle Nerve 1985;8:138–50
2. Hafler DA, Johnson D, Kelly JJ, et al. Monoclonal gammopathy and neuropathy: Myelin-associated glycoprotein reactivity and clinical characteristics. Neurology 1986;36:75–78
3. Steck AJ, Murray N, Dellagi K, et al. Peripheral neuropathy associated with monoclonal IgM autoantibody. Ann Neurol 1987;22:764–67
4. Latov N, Hays AP, Sherman WH. Peripheral neuropathy and anti-MAG antibodies. Crit Rev Neurobiol 1988;3:301–32
5. Smith IS. The natural history of chronic demyelinating neuropathy associated with benign IgM paraproteinaemia. A clinical and neurophysiological study. Brain 1994;117:949–57
6. Ellie E, Vital A, Steck A, et al. Neuropathy associated with "benign" anti–myelin-associated glycoprotein IgM gammopathy: Clinical, immunological, neurophysiological pathological findings and response to treatment in 33 cases. J Neurol 1996;243:34–43
7. Kuijf ML, Eurelings M, Tio-Gillen AP, et al. Detection of anti-MAG antibodies in polyneuropathy associated with IgM monoclonal gammopathy. Neurology 2009;73:688–95
8. Latov N. Pathogenesis and therapy of neuropathies associated with monoclonal gammopathies. Ann Neurol 1995;37:S32–S42
9. Steck AJ, Murray N, Justafre JC, et al. Passive transfer studies in demyelinating neuropathy with IgM monoclonal antibodies to myelin-associated glycoprotein. J Neurol Neurosurg Psychiatry 1985;48:927–29
10. Takatsu M, Hays AP, Latov N, et al. Immunofluorescence study of patients with neuropathy and IgM M proteins. Ann Neurol 1985;18:173–81
11. Tatum AH. Experimental paraprotein neuropathy, demyelination by passive transfer of human IgM anti–myelin-associated glycoprotein. Ann Neurol 1993;33:502–6
12. Vallat JM, De Mascarel HA, Bordessoule D, et al. Non-Hodgkin malignant lymphomas and peripheral neuropathies-13 cases. Brain 1995;118: 1233–45
13. Nobile-Orazio E, Gallia F, Terenghi F, et al. How useful are anti-neural IgM antibodies in the diagnosis of chronic immune-mediated neuropathies? J Neurol Sci 2008;266:156–63
14. Stalder AK, Eme B, Reimann R, et al. Immunoglobulin M deposition in cutaneous nerves of anti–myelin-associated glycoprotein polyneuropathy patients correlates with axonal degeneration. J Neuropathol Exp Neurol 2009;68:148–58
15. Nobile-Orazio E, Francomano E, Daverio R, et al. Anti-myelin-associated glycoprotein IgM antibody titers in neuropathy associated with macroglobulinemia. Ann Neurol 1989;26:543–50
16. Rebai T, Mhiri C, Heine P, et al. Focal myelin thickenings in a peripheral neuropathy associated with IgM monoclonal gammopathy. Acta Neuropathol 1989;79:226–32
17. Gabriel JM, Eme B, Bemasconi L, et al. Confocal microscopic localization of anti-myelin-associated glycoprotein autoantibodies in a patient with peripheral neuropathy initially lacking a detectable IgM gammopathy. Acta Neuropathol 1998;95:540–46
18. Sander S, Ouvrier RA, McLeod JG, et al. Clinical syndromes associated with tomacula or myelin swellings in sural nerve biopsies. J Neurol Neurosurg Psychiatry 2000;68:483–88
19. Vital A, Lagueny A, Julien J, et al. Chronic inflammatory demyelinating polyneuropathy associated with dysglobulinemia: A peripheral nerve biopsy study in 18 cases. Acta Neuropathol 2000;100:63–68
20. Cai Z, Cash K, Swift J, et al. Focal myelin swellings and tomacula in anti-MAG IgM paraproteinaemic neuropathy: Novel teased nerve fiber studies. J Peripher Nerv Syst 2001;6:95–101
21. Melmed C, Frail D, Duncan I, et al. Peripheral neuropathy with IgM kappa monoclonal immunoglobulin directed against myelin-associated glycoprotein. Neurology 1983;33:1397–405
22. Vital A, Vital C, Julien J, et al. Polyneuropathy associated with IgM monoclonal gammopathy. Immunological and pathological study in 31 patients. Acta Neuropathol 1989;79:160–67
23. Jacobs JM, Scadding JW. Morphological changes in IgM paraproteinaemic neuropathy. Acta Neuropathol 1990;80:77–84
24. Lach B, Rippstein P, Atack D, et al. Immunoelectron microscopic localization of monoclonal IgM antibodies in gammopathy associated with peripheral demyelinative neuropathy. Acta Neuropathol 1993;85:298–307
25. Vallat JM, Vital A, Magy L, et al. An update on nerve biopsy. J Neuropathol Exp Neurol 2009;68:833–44
26. Nobile-Orazio E, Vietorisz T, Messito MJ, et al. Anti-MAG IgM antibodies in patients with neuropathy and IgM M proteins: Detection by ELISA. Neurology 1983;33:939–42
27. Sobue G, Hashizume Y, Mukai E, et al. X-linked recessive bulbospinal neuronopathy. A clinicopathological study. Brain 1989;112:209–32
28. Koike H, Iijima M, Sugiura M, et al. Alcoholic neuropathy is clinicopathologically distinct from thiamine-deficiency neuropathy. Ann Neurol 2003;54:19–29
29. Koike H, Iijima M, Mori K, et al. Neuropathic pain correlates with myelinated fibre loss and cytokine profile in POEMS syndrome. J Neurol Neurosurg Psychiatry 2008;79:1171–79
30. Dyck PJ, Giannini C, Lais A. Pathologic alterations of nerves. In: Dyck PJ, Thomas PK, Griffin JW, et al, eds. *Peripheral Neuropathy*, 3rd ed. Philadelphia, PA: WB Saunders, 1993:514–95
31. Koike H, Misu K, Sugiura M, et al. Pathology of early- vs late-onset TTR Met30 familial amyloid polyneuropathy. Neurology 2004;63:129–38
32. Koike H, Iijima M, Mori K, et al. Nonmyelinating Schwann cell involvement with well-preserved unmyelinated axons in Charcot-Marie-Tooth disease type 1A. J Neuropathol Exp Neurol 2007;66:1027–36
33. Ohnishi A, Hirano A. Uncompacted myelin lamellae in dysglobulinemic neuropathy. J Neurol Sci 1981;51:131–40
34. Verhagen WI, Gabreëls-Festen AA, van Wensen PJ, et al. Hereditary neuropathy with liability to pressure palsies: A clinical, electroneurophysiological and morphological study. J Neurol Sci 1993;116:176–84
35. Hays AP, Latov N, Takatsu M, et al. Experimental demyelination of nerve induced by serum of patients with neuropathy and an anti-MAG IgM M-protein. Neurology 1987;37:242–56
36. Monaco S, Ferrari S, Bonetti B, et al. Experimental induction of myelin changes by anti-MAG antibodies and terminal complement complex. J Neuropathol Exp Neurol 1995;54:96–104
37. Meier C, Vandevelde M, Steck A, et al. Demyelinating polyneuropathy associated with monoclonal IgM-paraproteinaemia. Histological, ultrastructural and immunocytochemical studies. J Neurol Sci 1984;63:353–67

38. Martini R, Carenini S. Formation and maintenance of the myelin sheath in the peripheral nerve: Roles of cell adhesion molecules and the gap junction protein connexin 32. Microsc Res Tech 1998;41:403–15
39. Trapp BD, Andrews SB, Wong A, et al. Co-localization of the myelin-associated glycoprotein and the microfilament components, F-actin and spectrin, in Schwann cells of myelinated nerve fibres. J Neurocytol 1989;18:47–60
40. Lopate G, Kornberg AJ, Yue J, et al. Anti–myelin-associated glycoprotein antibodies: Variability in patterns of IgM binding to peripheral nerve. J Neurol Sci 2001;188:67–72
41. Steck AJ, Stalder AK, Renaud S. Anti–myelin-associated glycoprotein neuropathy. Curr Opin Neurol 2006;19:458–63
42. Hays AP, Lee SS, Latov N. Immune reactive C3d on the surface of myelin sheaths in neuropathy. J Neuroimmunol 1988;18:231–44
43. Monaco S, Bonetti B, Ferrari S, et al. Complement-mediated demyelination in patients with IgM monoclonal gammopathy and polyneuropathy. N Engl J Med 1990;322:649–52
44. Ferrari S, Morbin M, Nobile-Orazio E, et al. Antisulfatide polyneuropathy: Antibody-mediated complement attack on peripheral myelin. Acta Neuropathol 1998;96:569–74
45. Ritz MF, Erne B, Ferracin F, et al. Anti-MAG IgM penetration into myelinated fibers correlates with the extent of myelin widening. Muscle Nerve 1999;22:1030–37
46. Stoll G, Schmidt B, Jander S, et al. Presence of the terminal complement complex (C5b-9) precedes myelin degradation in immune-mediated demyelination of the rat peripheral nervous system. Ann Neurol 1991;30:147–55
47. Vallat JM, Tabaraud F, Sindou P, et al. Myelin widenings and MGUS-IgA: An immunoelectron microscopic study. Ann Neurol 2000;47:808–11
48. Vallat JM, Magy L, Sindou P, et al. IgG neuropathy: An immunoelectron microscopic study. J Neuropathol Exp Neurol 2005;64:386–90
49. de Waegh SM, Lee VM, Brady ST. Local modulation of neurofilament phosphorylation, axonal caliber, and slow axonal transport by myelinating Schwann cells. Cell 1992;68:451–63
50. Yin X, Crawford TO, Griffin JW, et al. Myelin-associated glycoprotein is a myelin signal that modulates the caliber of myelinated axons. J Neurosci 1998;18:1953–62
51. Lunn MP, Crawford TO, Hughes RA, et al. Anti–myelin-associated glycoprotein antibodies alter neurofilament spacing. Brain 2002;125:904–11
52. Dashiell SM, Tanner SL, Pant HC, et al. Myelin-associated glycoprotein modulates expression and phosphorylation of neuronal cytoskeletal elements and their associated kinases. J Neurochem 2002;81:1263–72

# IgM MGUS ANTI-MAG NEUROPATHY WITH PREDOMINANT MUSCLE WEAKNESS AND EXTENSIVE MUSCLE ATROPHY

YUICHI KAWAGASHIRA, MD,[1] NAOHIDE KONDO, MD,[1] NAOKI ATSUTA, MD, PhD,[1] MASAHIRO IIJIMA, MD, PhD,[1] HARUKI KOIKE, MD, PhD,[1] MASAHISA KATSUNO, MD, PhD,[1] FUMIAKI TANAKA, MD, PhD,[1] SUSUMU KUSUNOKI, MD, PhD,[2] and GEN SOBUE, MD, PhD[1]

[1] Department of Neurology, Nagoya University Graduate School of Medicine, Nagoya 466-8550, Japan
[2] Department of Neurology, Kinki University School of Medicine, Osaka, Japan

*Accepted 25 March 2010*

ABSTRACT: We report a patient with anti–myelin-associated glycoprotein (MAG) neuropathy, predominantly exhibiting severe motor symptoms, accompanied by extensive muscle atrophy mimicking Charcot–Marie–Tooth disease. Nerve conduction studies revealed mild retardation of motor conduction velocities and significant prolongation of distal latency. Sural nerve biopsy revealed widely spaced myelin and positive staining of myelinated fibers with an IgM antibody. Predominant motor symptoms with muscle atrophy can be one of the clinical manifestations of anti-MAG neuropathy.

*Muscle Nerve* **42:** 433–435, 2010

Myelin-associated glycoprotein (MAG) is a minor component of the myelin membrane that plays an important role in axon–Schwann-cell interaction.[1–3] More than 50% of patients with neuropathy-associated IgM monoclonal gammopathy possess antibodies against MAG.[4]

Neuropathy associated with IgM monoclonal gammopathy of undetermined significance (MGUS) with an antibody against MAG represents a distinctive clinical syndrome characterized by male predominance, late age of onset, slow progression, predominantly sensory symptoms, and, in particular, the pronounced loss of deep sensation with sensory ataxia.[4–9] Conversely, predominant motor impairment has been reported only on occasion.[7,10] Herein, we report a patient with anti-MAG neuropathy presenting with predominantly motor symptoms and extensive muscle atrophy of the lower limbs, mimicking Charcot–Marie–Tooth (CMT) disease.

## CASE REPORT

A 62-year-old man was admitted with distal muscle weakness of the lower limbs, which was accompanied by marked muscle atrophy. He did not have a notable individual or family history, and there were no growth problems during his infancy. Muscle weakness of the bilateral toes began approximately 5 years prior to our clinical evaluation, along with slow progression in the bilateral lower limbs. Muscle atrophy of the lower limbs gradually became conspicuous. In addition, mild paresthesia in the distal portion of the lower limbs developed over the last 2 years. On admission, neurological examination revealed bilateral severe muscle weakness and extensive muscle atrophy, predominantly in the distal portion of the legs (Fig. 1A). Manual muscle testing, recorded in the lower legs, was level 1. Neither muscle weakness nor muscle atrophy was observed in the upper extremities. Touch, pain, vibratory, and joint sensations of all extremities were mildly reduced in a glove-and-stocking distribution Pseudoathetosis was not observed in the hand. A Romberg sign could not be determined because the patient could not remain standing unaided. There were no abnormalities in the cranial nerves and autonomic nervous system. Deep tendon reflexes were absent on both sides of the legs and arms.

In routine laboratory examinations, we found that the serum IgM level was significantly elevated to 890 mg/dl (normal 35–220 mg/dl), and IgM-kappa–type M-protein was identified by serum immune electrophoresis. Western blotting confirmed positive serum anti-MAG IgM antibody. In addition, sulfoglucuronyl paragloboside (SGPG) IgM antibody titer was also significantly elevated, based on the results of an enzyme-linked immunosorbent assay. In contrast, serum IgM and IgG antibodies to GM1, GM2, GM3, GD1a, GD1b, GD3, GT1b, GQ1b, GA1, Gal-c were all negative.[11] Analysis of cerebrospinal fluid showed that protein content was increased significantly at 380 mg/dl (normal range 15–45 mg/dl), whereas cell count was normal. The ratio of plasma cells in the bone marrow was less than 5%, and no lymphoplasmacytoid elements were evident.

Motor nerve conduction studies in the median and ulnar nerve revealed mild retardation of 42 m/s and 43 m/s, respectively. Significant prolongations of distal latency in the median and ulnar nerve were highly conspicuous, at 13.2 ms and 5.7 ms, respectively. Compound muscle action potential amplitudes in the median and ulnar nerve were 4.4 mV and 5.8 mV, respectively. Motor and sensory

**Abbreviations:** CIDP, chronic inflammatory demyelinating polyneuropathy; CMT, Charcot–Marie–Tooth; IVIg, intravenous immunoglobulin; MAG, myelin-associated glycoprotein; MGUS, monoclonal gammopathy of undetermined significance; MRI, magnetic resonance imaging; SGPG, sulfoglucuronyl paragloboside; WSM, widely spaced myelin

**Key words:** MGUS, MA, peripheral neuropathy, weakness, muscle atrophy

**Correspondence to:** G. Sobue; e-mail: sobueg@med.nagoya-u.ac.jp



Published online 15 August 2010 in Wiley InterScience (www.interscience.wiley.com). DOI 10.1002/mus.21741

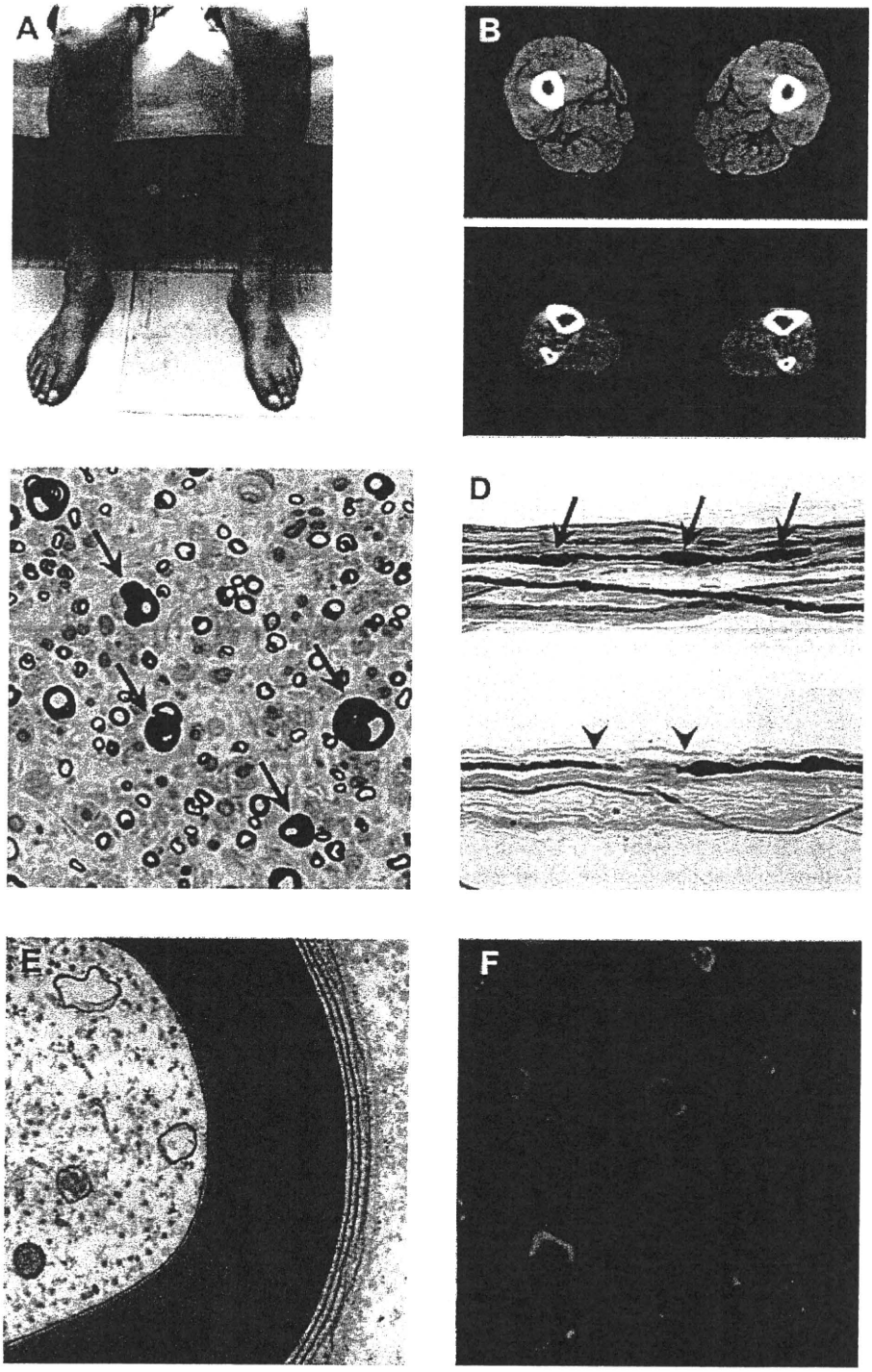


**FIGURE 1. (A)** The patient's lower extremities. Bilateral lower legs are visibly atrophic. **(B)** Muscle computed tomography of the lower extremities. Muscle atrophy predominant in the lower legs (lower panel) is evident. **(C)** Transverse section of a sural nerve biopsy stained with toluidine blue. Fibers with redundant myelin loops are observed (arrows). **(D)** Teased fibers show tomacula (arrows) and segmental demyelination (arrowheads). **(E)** Electron micrographs of the transverse section. Widely spaced myelin is observed in some outer lamellae of the myelin sheath. **(F)** Immunofluorescence study of cross-sections. The immune reaction with IgM antibody is positive on the myelin sheath. [Color figure can be viewed in the online issue, which is available at www.interscience.wiley.com.]

nerve conduction studies in the lower limbs and sensory nerve conduction studies in the upper limbs were not elicited at all. Magnetic resonance imaging (MRI) suggesting spinal disorders was not seen in the spinal cord and the cauda equina was not enhanced with gadolinium. Computed

tomography revealed muscle atrophy in the bilateral lower legs (Fig. 1B). Sural nerve biopsy revealed a moderate decrease in myelinated fiber density, predominantly large myelinated fibers (3410 fibers/mm$^2$), axonal atrophy, and redundant myelin loops (Fig. 1C). We did not detect vasculitis or infiltration of inflammatory cells, or amyloid deposition in the endoneurium, which would have been be revealed by Congo red staining. The frequency of segmental demyelination and tomacula in teased-fiber preparations was 12.5% and 10.8%, respectively (Fig. 1D). Widely spaced myelin (WSM) was detected by electron microscopy, and the frequency of one in the myelinated fibers was 17.2% (Fig. 1E). Indirect immunofluorescence for human IgM antibody was positive on myelinated fibers (Fig. 1F).

Based on the laboratory, electrophysiological, and pathological findings, we diagnosed our patient with anti-MAG neuropathy. He was treated with intravenous immunoglobulin (IVIg) therapy and showed clinical improvement. Although he could not remain standing without support prior to IVIg therapy, he was able to walk with a cane thereafter.

## DISCUSSION

In this case report we have presented a patient with anti-MAG neuropathy that manifested predominant muscle weakness and extensive muscle atrophy of the lower legs, which is a rare form in this neuropathy. Although muscle weakness is often observed in the distal portion of the lower limbs in patients with anti-MAG neuropathy, it rarely overshadows the sensory features and gait disturbance usually dependent on the sensory ataxia.[8,9,12] Sensorimotor neuropathy with severe weakness in the presence of IgM MGUS was described by Ellie et al.[7] However, all of their patients had severe sensory ataxia and a high ataxic score in addition to muscle weakness, whereas the impairment of deep sensation in our case was mild. Predominant motor symptoms may characterize the features of CMT, chronic inflammatory demyelinating polyradiculoneuropathy (CIDP), and lumbosacral plexopathy. The characteristic features of nerve conduction studies in anti-MAG neuropathy include marked prolongation of distal motor latencies disproportionate to proximal segment conduction velocities, indicating predominantly distal demyelination in contrast to CIDP and CMT.[13] In addition, muscle atrophy was observed in the distal, but not proximal, portion of the lower extremities, and painful symptoms were also not reported. These findings are atypical in lumbosacral plexopathy.[14] Pathological findings further support the view that the pathogenesis of neuropathy in this patient was due to IgM monoclonal gammopathy for the antibody against MAG/SGPG.

Previous reports have revealed that the IgM from patients with neuropathy associated with IgM monoclonal gammopathy could recognize a shared epitope between MAG and glycoconjugates such as SGPG.[10,15] Cross-reactivity between anti-MAG antibody with HNK-1 epitope and other glycoconjugates may be responsible for wide immunoreactivity and may be the reason for the differing clinical manifestations. Predominant motor symptoms and muscle atrophy can be one of the clinical manifestations of anti-MAG neuropathy. Consequently, careful differential diagnosis is necessary for patients with predominant motor neuropathy, especially those with IgM monoclonal gammopathy.

## REFERENCES


1. Martini R, Schachner M. Molecular bases of myelin formation as revealed by investigations on mice deficient in glial cell surface molecules. Glia 1997;19:298–310.
2. Lopate G, Kornberg AJ, Yue J, Choksi R, Pestronk A. Anti-myelin associated glycoprotein antibodies: variability in patterns of IgM binding to peripheral nerve. J Neurol Sci 2001;188:67–72.
3. Lunn MP, Crawford TO, Hughes RA, Griffin JW, Sheikh KA. Anti-myelin-associated glycoprotein antibodies alter neurofilament spacing. Brain 2002;125:904–911.
4. Latov N. Pathogenesis and therapy of neuropathies associated with monoclonal gammopathies. Ann Neurol 1995;37(suppl):S32–42.
5. Mendell JR, Sahenk Z, Whitaker JN, Trapp BD, Yates AJ, Griggs RC, et al. Polyneuropathy and IgM monoclonal gammopathy: studies on the pathogenetic role of anti-myelin-associated glycoprotein antibody. Ann Neurol 1985;17:243–254.
6. Vital A, Vital C, Julien J, Baquey A, Steck AJ. Polyneuropathy associated with IgM monoclonal gammopathy. Immunological and pathological study in 31 patients. Acta Neuropathol 1989;79:160–167.
7. Ellie E, Vital A, Steck A, Boiron JM, Vital C, Julien J. Neuropathy associated with "benign" anti-myelin-associated glycoprotein IgM gammopathy: clinical, immunological, neurophysiological and pathological findings and response to treatment in 33 cases. J Neurol 1996;243:34–43.
8. Chassande B, Léger JM, Younes-Chennoufi AB, Bengoufa D, Maisonobe T, Bouche P, et al. Peripheral neuropathy associated with IgM monoclonal gammopathy: correlations between M-protein antibody activity and clinical/electrophysiological features in 40 cases. Muscle Nerve 1998;21:55–62.
9. Nobile-Orazio E, Manfredini E, Carpo M, Meucci N, Monaco S, Ferrari S, et al. Frequency and clinical correlates of anti-neural IgM antibodies in neuropathy associated with IgM monoclonal gammopathy. Ann Neurol 1994;36:416–424.
10. Kusunoki S, Craft JE, Roach B, Hardin JA, Yu RK. Neuropathy and IgM paraproteinemia: differential binding of IgM M-proteins to peripheral nerve glycolipids. Neurology 1987;37:1795–1797.
11. Kusunoki S, Chiba A, Kon K, Ando S, Arisawa K, Tate A, et al. N-acetylgalactosaminyl GD1a is a target molecule for serum antibody in Guillain–Barré syndrome. Ann Neurol 1994;35:570–576.
12. Yeung KB, Thomas PK, King RH, Waddy H, Will RG, Hughes RA, et al. The clinical spectrum of peripheral neuropathies associated with benign monoclonal IgM, IgG and IgA paraproteinaemia. Comparative clinical, immunological and nerve biopsy findings. J Neurol 1991;238:383–391.
13. Kaku DA, England JD, Sumner AJ. Distal accentuation of conduction slowing in polyneuropathy associated with antibodies to myelin-associated glycoprotein and sulphated glucuronyl paragloboside. Brain 1994;117:941–947.
14. Dyck PJ, Norell JE, Dyck PJ. Non-diabetic lumbosacral radiculoplexus neuropathy: natural history, outcome and comparison with the diabetic variety. Brain 2001;124:1197–1207.
15. Weiss MD, Dalakas MC, Lauter CJ, Willison HJ, Quarles RH. Variability in the binding of anti-MAG and anti-SGPG antibodies to target antigens in demyelinating neuropathy and IgM paraproteinemia. J Neuroimmunol 1999;95:174–184.

Clinical Neurology and Neurosurgery xxx (2011) xxx–xxx

Contents lists available at ScienceDirect

Clinical Neurology and Neurosurgery

journal homepage: www.elsevier.com/locate/clineuro

Case report

# Central nervous system involvement in n-hexane polyneuropathy demonstrated by MRI and proton MR spectroscopy

A. Hashizume[a], H. Koike[a], Y. Kawagashira[a], H. Banno[a,b], K. Suzuki[a], M. Ito[a], M. Katsuno[a,b], H. Watanabe[a], F. Tanaka[a], S. Naganawa[c], R. Kaneko[d], A. Ishii[d], G. Sobue[a,*]

[a] Department of Neurology, Nagoya University Graduate School of Medicine, 65 Tsurumai-cho, Showa-ku, Nagoya 466-8550, Japan
[b] Institute for Advanced Research, Nagoya University, Nagoya, Japan
[c] Department of Radiology, Nagoya University Graduate School of Medicine, Nagoya, Japan
[d] Department of Legal Medicine and Bioethics, Nagoya University Graduate School of Medicine, Nagoya, Japan

ARTICLE INFO

*Article history:*
Received 31 August 2009
Received in revised form 19 January 2011
Accepted 22 January 2011
Available online xxx

*Keywords:*
n-Hexane
Polyneuropathy
Central nervous system
Magnetic resonance spectroscopy
Lactate peak

## 1. Introduction

The organic solvent n-hexane is a well-described causal agent in polyneuropathy. Although most cases of n-hexane polyneuropathy result from industrial exposure to glues containing the chemical, some are caused by addictive inhalation. In abuse cases, neurological manifestations are generally severe because of the high intensity of exposure.

n-Hexane polyneuropathy has two characteristic electrophysiological features: conduction block and conduction slowing. Nerve biopsy specimens show primarily axonal swelling as well as secondary paranodal myelin retraction and myelin thinning, which may underlie the electrophysiological features [1]. In contrast to toluene toxicity, the damage caused by n-hexane has been considered to be mostly restricted to peripheral nerves [2]. Although many cases of peripheral neuropathy due to n-hexane toxicity have been reported, central nervous system (CNS) involvement has not been fully described in humans, although it has been observed in animal models [3]. A previous electrophysiological study suggested the presence of CNS lesions by evoked potential abnormalities [4].

In the present report, we describe a patient with n-hexane polyneuropathy with CNS lesions using magnetic resonance imaging (MRI) and proton magnetic resonance spectroscopy ($^1$H MRS).

## 2. Case report

A 51-year-old woman complained of difficulty rising up from a seated position and climbing stairs for six months prior to admission to our hospital. Her symptoms gradually worsened until she could not rise up at all for the month before admission. She had no past or family history of neurological disorders. A neurological examination disclosed no impairment of consciousness. Cranial nerves were normal. Severe bilateral muscle weakness was present. Her grip power was almost zero in both hands. Although touch, pain, and temperature sensations were nearly normal objectively, she felt discomfort described as "walking on sand" on the soles of her feet. Vibration sensations in her lower legs were moderately decreased. Deep tendon reflexes were absent in the upper and lower extremities. Plantar responses were flexor on both sides.

All routine hematological, serological and biochemical examinations were normal. Cerebrospinal fluid examination revealed no abnormalities in cell count or protein level, including myelin basic protein and oligoclonal band. A nerve conduction study (NCS) revealed conduction slowing with conduction block in both motor

* Corresponding author. Tel.: +81 52 744 2385; fax: +81 52 744 2384.
*E-mail address:* sobueg@med.nagoya-u.ac.jp (G. Sobue).

0303-8467/$ – see front matter 
doi:10.1016/j.clineuro.2011.01.008

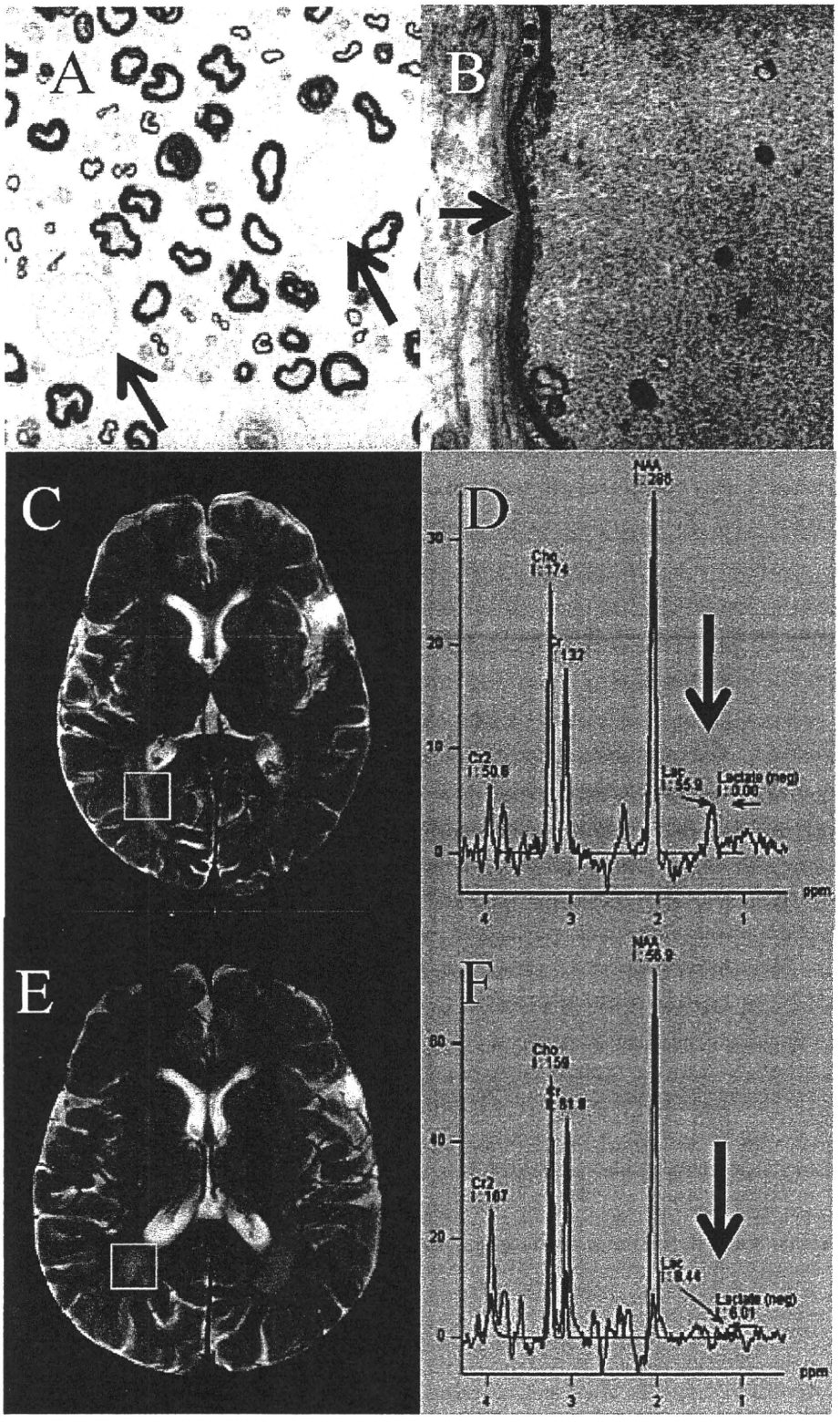


**Fig. 1.** Sural nerve specimen, head MRI, and proton MR spectroscopy. (A) Light micrograph of transverse section of a sural nerve biopsy specimen showing swollen axons with no or extremely thin myelin (arrow). (B) Electron micrograph showing a giant axon with extremely thin myelin caused by accumulating neurofilaments (arrow). (C) Head T2-weighted MRI image showing a high intensity area of white matter around the cornua of the lateral ventricle. The open white square denotes the region of interest for proton magnetic resonance spectroscopy ($^1$H MRS). (D) $^1$H MRS showing an abnormal lactate peak (arrow). Although the high intensity area of white matter remained at about the same level (E), the abnormal lactate peak returned to normal in the $^1$H MRS (F).

Please cite this article in press as: Hashizume A, et al. Central nervous system involvement in n-hexane polyneuropathy demonstrated by MRI and proton MR spectroscopy. Clin Neurol Neurosurg (2011), doi:10.1016/j.clineuro.2011.01.008

and sensory nerves. The compound muscle potential (CMAP), the distal latency (DL), and the motor conduction velocity (MCV) on tibial nerve were 0.6 mV, 10 ms, and 25 m/s, respectively. Sural nerve response could not be elicited. Electromyograms of left tibialis anterior muscle revealed many polyphasic and long duration waveforms. No abnormalities were detected in cervical, thoracic, and lumbar MRI scans.

A nerve biopsy was performed on the left sural nerve. A transverse section of the specimen showed conspicuously swollen axons (Fig. 1A). Although a light microscopic examination did not show any myelin on these swollen axons, electron micrographs revealed an extremely thin myelin layer (Fig. 1B). In addition, a marked accumulation of neurofilaments was observed in the axons. Teased fibers also showed axonal swelling with demyelination or extremely thin myelin. Based on these clinical, electrophysiological, and nerve pathological findings, we suspected the patient as having n-hexane polyneuropathy.

A careful interview with the patient revealed that she bought large amounts of stain remover that contained n-hexane and its isomer (n-hexane 62%, isohexane 25%, metylcyclopentane 13%, others <1%). She had inhaled the solvent addictively for numerous years. She used no other organic solvents. The result of gas chromatograph/mass spectrometry (GC/MS) showed no detectable level of toluene or ethylbenzene.

The patient then underwent cranial MRI and single-voxel $^{1}$H MRS on a 1.5-T system (General Electric Signa Infinity HiSpeed SR77, Block Imaging International, Lansing, MI, USA), equipped with a circularly polarized head coil. The MRI protocol included sagittal T1-weighted fluid attenuated inversion recovery (FLAIR; TR, 10,000 ms; TI, 560 ms; TE, 85 ms) and axial T2-weighted fast spin echo (FSE; TR, 4250 ms; TE, 190 ms; ETL, 24 ms) images. Slice thickness was 4 mm, field of view was 24 cm × 24 cm, and matrix size was 320 × 256. $^{1}$H MR spectroscopy provided spectra peak areas at 2.0, 3.0, and 3.2 ppm, corresponding to n-acetylaspartate (NAA), creatine (Cr), and choline (Cho). The NAA/Cr, NAA/Cho, and Cho/Cr ratios were analyzed using SAGE (GE Medical Systems, Waukesha, WI, USA). Brain MRI T2-weighted images revealed a high intensity area of white matter around the cornua of the lateral ventricle (Fig. 1C). $^{1}$H MRS demonstrated a significant increase in the lactate peak (Fig. 1D). In a brainstem auditory evoked potential (BAEP) study, absolute latencies of I, III, and V were 1.66 ms, 4.16 ms, and 6.36 ms, respectively (normal values [mean ± SD]: 1.7 ± 0.15, 3.9 ± 0.19, and 5.7 ± 0.25, respectively). Thus, the I–III, III–V, and I–V interpeak latencies were 2.50 ms, 2.20 ms, and 4.70 ms, respectively (normal values: 2.1 ± 0.15, 1.9 ± 0.18, and 4.0 ± 0.23, respectively). In a visual evoked potentials (VEPs) study, right and left P100 latency were also prolonged to 122 ms and 117 ms, respectively (normal values: 102.3 ± 5.1). Central nervous conduction times calculated by these results were mildly prolonged.

With no treatment, the patient's muscle strength gradually improved after admission. One month later, she could rise up by herself and her grip power recovered to 5–10 kg W. Although the discomfort in her soles continued to worsen for two more months, it began to improve thereafter. Six months later, the deep tendon reflexes in her lower extremities returned to the normal range. The NCS findings also gradually recovered. CMAP, DL, and MCV on tibial nerve of 10 months after cessation of inhalation were 6.6 mV, 5.0 ms, and 35 m/s, respectively. The sensory nerve action potential and the sensory conduction velocity of sural nerve were 10.1 μV and 44 m/s, respectively. Although the high intensity area of white matter seen in the brain MRI T2-weighted images remained at about the same level six months later (Fig. 1E), the abnormal lactate peak returned to almost normal in the $^{1}$H MRS during the clinical discovery (Fig. 1F).

## 3. Discussion

In this report, we described a patient with a CNS lesion probably due to n-hexane polyneuropathy. The axonal swelling seen in the sural nerve biopsy specimen, the characteristic nerve conduction studies showing both conduction block and conduction slowing, and the improvement of symptoms upon cessation of inhalation, all point to addictive inhalation of n-hexane as the cause of this patient's polyneuropathy. The CNS lesion demonstrated by $^{1}$H MRS also showed clear improvement after n-hexane inhalation was stopped. The use of other organic solvents such as toluene, which can induce CNS lesions, was ruled out based on the GC/MS results.

The most striking aspect of this case was the CNS involvement. The cerebral MRI T2-weighted images showed an abnormally high-intensity area around the lateral ventricle. In addition, $^{1}$H MRS revealed abnormal, but reversible, lactate peaks. Multiple sclerosis and age-related factors should be considered in the differential diagnosis. However, the patient did not show an elevation of myelin basic protein or oligoclonal band in the cerebrospinal fluid or in any MRI findings in the spinal cord. In addition, an increase in the Cho/Cr ratio or the presence of a lactate peak has not been reported to occur in the white matter of the ageing brain. For these reasons, we conclude that the observed CNS changes were due to n-hexane. The fact that six months after ceasing n-hexane inhalation, the abnormal lactate peaks disappeared strongly supports this conclusion.

Several other reports have suggested CNS effects due to n-hexane inhalation. Oge et al. described a central nerve conduction delay using the electrophysiological method of transcranial magnetic stimulation [5]. Moreover, studies using patterned visual evoked potential (pVEP), brainstem auditory evoked potential (BAEP), and somatosensory evoked potential (SEP) have suggested subclinical central nerve involvement in n-hexane neuropathy [2]. They concluded that there were chronic neurotoxic effects of n-hexane on the CNS, including the cerebrum, the brainstem, and the spinal cord. In addition, Spencer et al. demonstrated a pathological change in the CNS in experimental animals [3]. They reported that light microscopic observation of CNS tissue obtained from rats and cats revealed abnormally large fibers with swollen axons and myelin sheaths inappropriately thin for their diameter. If similar pathological change occurred in the CNS of our patient, the CNS findings demonstrated by MRI or MR spectroscopy we obtained were explainable.

The present case study represents a new line of evidence of CNS involvement in n-hexane polyneuropathy.

## References

[1] Kuwabara S, Kai MR, Nagase H, Hattori T. n-Hexane neuropathy caused by addictive inhalation: clinical and electrophysiological features. Eur Neurol 1999;41:163–7.
[2] Chang AP, England JD, Garcia CA, Sumner AJ. Focal conduction block in n-hexane polyneuropathy. Muscle Nerve 1998;21:964–9.
[3] Spencer PS, Schaumburg HH. Ultrastructual studies of the dying-back process. Differential vulnerabilities of PNS and CNS fibers in experimental central–peripheral distal axonopathies. Neuropathol Exp Neurol 1977;36:300–20.
[4] Chang YC. Neurotoxic effects of n-hexane on the human central nervous system: evoked potential abnormalities in n-hexane polyneuropathy. J Neurol Neurosurg Psychiatry 1987;50:269–74.
[5] Oge AM, Yazici J, Boyaciyan A, Eryildiz D, Ornek I, Konyalioglu R, et al. Peripheral and central conduction in n-hexane polyneuropathy. Muscle Nerve 1994;17:1416–30.

Please cite this article in press as: Hashizume A, et al. Central nervous system involvement in n-hexane polyneuropathy demonstrated by MRI and proton MR spectroscopy. Clin Neurol Neurosurg (2011), doi:10.1016/j.clineuro.2011.01.008